

Hierarchical Cell-Free Massive MIMO: A Simplified Design for Uniform Service Quality

Wei Jiang, *Senior Member, IEEE* and Hans Dieter Schotten

Abstract—In traditional cellular networks, users at the cell edge often suffer from poor quality of service (QoS) due to large distance-dependent path loss and severe inter-cell interference. While cell-free (CF) massive multi-input multi-out (MIMO) mitigates this issue by distributing access points (APs) to ensure uniform QoS, the deployment of numerous distributed APs and a fronthaul network incurs high infrastructure costs. To balance performance and cost efficiency, this article proposes a simplified design called hierarchical cell-free (HCF) massive MIMO. The key idea is to reduce the number of APs, thus minimizing the scale of the fronthaul network. The antennas from the decommissioned APs are aggregated at a central base station (cBS), which also serves as the coordinator for distributed APs. We derive closed-form expressions for uplink and downlink spectral efficiency (SE) for HCF, CF, and cellular massive MIMO under pilot contamination and correlated fading channels, considering the use of multi-antenna APs. Numerical results confirm that the hierarchical architecture achieves 95%-likely per-user SE comparable to CF, enhancing cell-edge user rates in cellular systems by over 100 times, while significantly reducing the complexity and cost of the fronthaul network in CF. We develop max-min fairness algorithms for joint power control of the cBS and APs in the downlink, and the users in the uplink. These algorithms not only boost fairness and system capacity but also dramatically lower transmission power, e.g., achieving over 70% savings in uplink, particularly beneficial for battery-powered mobile devices.

Index Terms—Cell-free massive MIMO, cell edge, correlated channels, cost-effectiveness, energy efficiency, fronthaul overhead, pilot contamination, max-min power control

I. INTRODUCTION

In traditional cellular networks, each cell is served by a base station (BS) positioned at its center. Users close to the BS generally experience high quality of service (QoS). Conversely, users at the cell edge often encounter poor QoS due to factors such as large signal attenuation over distance, severe interference from neighboring cells, and handover inefficiencies inherent to cellular systems [2]. As outlined in the ITU-R M.2410 recommendation [3], the peak spectral efficiency (SE) targets for fifth-generation (5G), typically achieved in the cell center, are set at 30 bps/Hz in the downlink and 15 bps/Hz in the uplink. In contrast, the 95%-likely SE [4] — also known as the 5th percentile user rate [5] or 5%-outage rate — serves as a key metric for evaluating cell-edge performance [6]. 5G's targets for this metric are

Part of this work was presented at the 2024 IEEE International Conference on Communication (ICC-2024) [1]. (Corresponding author: Wei Jiang)

W. Jiang and H. D. Schotten are with the German Research Center for Artificial Intelligence (DFKI), Kaiserslautern, Germany, and are also with University of Kaiserslautern (RPTU), Paul-Ehrlich Street, Kaiserslautern, 67663 Germany (e-mail: wei.jiang@dfki.de; schotten@eit.uni-kl.de).

notably lower, set at 0.3 bps/Hz (downlink) and 0.21 bps/Hz (uplink) in indoor hotspots, further reduced to 0.12 bps/Hz and 0.0453 bps/Hz, respectively, in rural areas. This stark contrast reveals a substantial performance gap, over a 100-fold difference, between users at the cell center and edge, underscoring the critical need for improved cell-edge QoS in next-generation networks [7].

Cell-free (CF) massive multi-input multi-output (MIMO) has arisen as a groundbreaking approach in cellular network design, attracting much attention from both academia and industry [8]. Departing from conventional cell-based structures, CF deploys a large number of distributed access points (APs) spread throughout the coverage area. These APs, coordinated by a central processing unit (CPU) via a fronthaul network, work collaboratively to provide uniform QoS to all users. Many advancements in CF massive MIMO technology have been achieved in recent years. Early work by Ngo et al. [5] validated its ability to effectively mitigate the cell-edge problem and ensure uniform QoS by benchmarking the 95%-likely user rate against small-cell systems. Concurrently, Nayebi et al. [4] evaluated downlink performance under different linear precoding and power allocation algorithms. To address scalability challenges, Björnson et al. [9] systematically reviewed dynamic cooperation clustering and network densification limits. Interdonato et al. [10] later demonstrated that the use of downlink pilots can improve performance despite introducing overhead and exacerbating pilot contamination. In [11], Ngo et al. developed an optimization method to maximize total energy efficiency under per-user SE and per-AP power constraints. Björnson and Sanguinetti [12] provided a comprehensive analysis under four levels of uplink cooperation, revealing the advantage of centralized minimum mean-square error (MMSE) processing.

While CF offer the potential for improved performance and fairness, the deployment of numerous distributed APs and a fronthaul network incurs high infrastructure costs. Traditional wireless networks already face high deployment costs and challenges related to site acquisition. CF systems exacerbate these issues by requiring hundreds of wireless AP sites in a small area [13]. Additionally, installing and operating a large-scale fronthaul network, typically based on fiber-optic cables, to connect a massive number of APs leads to substantial capital and operational costs and may face deployment restrictions in certain areas. Recent research has proposed several strategies to overcome this obstacle, with key approaches focusing on the fronthaul network. For instance, Furtado et al. [14] discussed the challenges of a non-scalable complex and costly fronthaul network and identified

cost-saving fronthaul topologies. Buzzi et al. proposed user-centric approaches [15], [16] that reduce fronthaul overhead by dynamically clustering APs around users, maintaining performance with reduced complexity. Infrastructure costs can also be optimized through AP design: Jiang and Schotten [17] demonstrated that equipping APs with multiple antennas reduces the total number of required wireless AP sites, thereby lowering fronthaul costs.

Wireless fronthaul alternatives have emerged as viable solutions to eliminate the high costs associated with infrastructure construction, such as trenching, fiber cable laying, and life-cycle maintenance. Demirhan and Alkhateeb [18] proposed to replace optical fiber fronthaul with millimeter-wave wireless fronthaul to minimize infrastructure costs and deployment time. Similarly, Jazi et al. [19] explored integrated access and backhaul via spectrum sharing, optimizing fronthaul efficiency in dense networks. For industrial settings, Li et al. [20] introduced a two-tier terahertz fronthaul architecture, eliminating wired connections in indoor CF deployments. The challenges under constrained fronthaul capacity have also driven innovations in signal processing. For instance, Kim et al. [21] proposed a precoding scheme with max-min power allocation using fronthaul compression and low-resolution digital-to-analog converters. Parida and Dhillon [22] quantified the impact of finite fronthaul capacity on downlink performance, motivating advanced quantization techniques such as scalable multivariate compression [23]. Ranjbar et al. [24] further analyzed sequential topologies (e.g., daisy chains) under hardware limitations, emphasizing trade-offs between memory constraints and optimal design. Resource allocation strategies, such as meta-heuristic bit allocation frameworks [25], have also been developed to maximize fronthaul efficiency under strict capacity limits.

Wireless backhauling is by far the most cost-effective solution, but its adoption does not come for free [26]. *Out-of-band* implementations require each AP to be equipped with an additional transceiver and antenna or antenna array. Also, it potentially incurs regulatory licensing fees for the specific frequency band. Conversely, *in-band* frequency usage requires the access link to allocate approximately half of its frequency/time resources to the fronthaul link, significantly degrading system performance. To optimize the cost-effectiveness, this article proposes a simplified design called hierarchical cell-free (HCF) massive MIMO. Our design deliberately reduces the number of APs so as to minimize the scale of the fronthaul network. The antennas from the decommissioned APs are aggregated to a centrally located BS, which we refer to as the central base station (cBS) to distinguish it from the traditional paradigm. As the antennas and transceivers are reused from the retired APs, HCF avoids additional hardware costs. The cBS not only serves as a central signal transceiver but also replaces the CPU in CF systems to coordinate the distributed APs.

The main contributions of this work can be listed as follows:

- This article is the first to introduce a hierarchical pattern that smoothly bridges the gap between fully centralized (cellular) and fully distributed (CF) massive MIMO.

Through limiting the number of distributed APs, it effectively lowers the scale of the fronthaul network, thus reducing complexity and cost. cBS is introduced to retain the centralization gain without incurring deployment costs, as it repurposes hardware from the decommissioned APs.

- We develop HCF max-min fairness algorithms for joint power control of the cBS and APs in the downlink, and the users in the uplink. These power controls not only enhance fairness and system capacity but also substantially save the transmission power.
- We derive closed-form SE expressions for not only HCF, but also CF and cellular, in both downlink and uplink operations. Our analysis accounts for multi-antenna APs, spatially correlated channels, and pilot contamination. It extends beyond prior CF works, which were mostly constrained to single-antenna APs or independent channels.
- Comprehensive numerical evaluation is conducted to compare HCF, CF, and cellular massive MIMO in both uplink and downlink, considering key performance metrics including 95%-likely per-user SE (fairness), sum throughput (capacity), and power saving (energy efficiency), while accounting for various factors, such as micro vs. macro cells, pilot contamination, angular spread, and equal/max-min power optimization.

The paper is organized as follows: Section II models the HCF system. Section III discusses uplink training in the context of channel correlation and pilot contamination. Section IV analyzes uplink data transmission, deriving closed-form SE expressions and proposing max-min power optimization. Section V extends this analysis to downlink transmission. Section VI details the simulation setups and presents key numerical results. Finally, Section VII offers conclusions.

Notations: Throughout this article, **boldface** lowercase and uppercase letters denote vectors and matrices, respectively. The following operators are used for their operations: $(\cdot)^*$ (conjugate), $(\cdot)^T$ (transpose), $(\cdot)^H$ (Hermitian transpose), $(\cdot)^{-1}$ (inverse), and $\text{tr}(\cdot)$ (the trace of a matrix). The Frobenius norm is represented by $\|\cdot\|$, \log_2 specifies a logarithm with base 2, and \lg is the common logarithm with base 10. Statistical expectation is denoted by \mathbb{E} , and \mathbf{I} refers to an identity matrix of suitable dimensions. The symbol \in indicates set membership, while \setminus represents the set difference, e.g., $k' \in \mathbb{K} \setminus \{k\}$ means k' is an element of the set \mathbb{K} excluding the specific element k . Estimated variables are marked with a hat (e.g., \hat{x}), and estimation errors are distinguished by a tilde (e.g., \tilde{x}). The notation \mathcal{CN} corresponds to a complex Gaussian distribution.

II. SYSTEM MODEL

In CF massive MIMO, a network of M massive antennas is distributed across a coverage area to serve K users, as depicted in Fig.1a. To exploit the advantages of channel hardening and favorable propagation [27], the number of service antennas must substantially exceed the number of users, i.e., $M \gg K$. User equipment (UE) is typically equipped with a single antenna, while each AP may have either a

single or multiple antennas. A CPU manages all APs via a fronthaul network. In this paper, we consider a hierarchical design for CF massive MIMO, as shown in Fig. 1b. The proposed architecture features a cBS with N_b co-located antennas, positioned near the center of the coverage area. The network also includes L distributed APs, each equipped with N_a antennas. To distinguish from the conventional paradigm, these are referred to as edge access points (eAPs) hereinafter. Unlike conventional base stations, the cBS also functions as the CPU for coordinating the eAPs. We assume that HCF maintains the same total number of antennas as CF, such that $N_b + L N_a = M$. The aim of this design is to simplify the fronthaul network, thus lowering complexity and cost, as only a subset of the service antennas require connections.

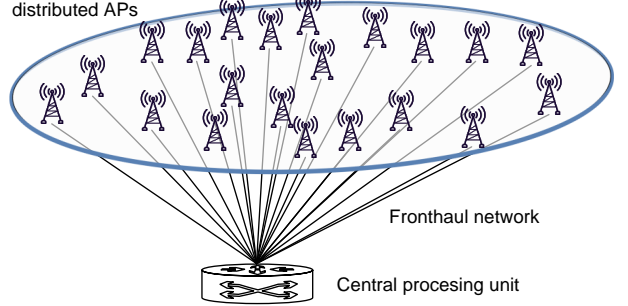
The index sets of eAPs and users are denoted by $\mathbb{L} = \{1, \dots, L\}$ and $\mathbb{K} = \{1, \dots, K\}$, respectively. The channel between eAP l , $\forall l \in \mathbb{L}$ and user k , $\forall k \in \mathbb{K}$ is denoted by $\mathbf{h}_{kl} \in \mathbb{C}^{N_a}$. Under the standard block fading model, each *coherent block* is a time-frequency interval of τ_c channel uses during which the channel response remains approximately constant. Each coherence block applies an independent realization from a *correlated*¹ Rayleigh fading distribution $\mathbf{h}_{kl} \sim \mathcal{CN}(\mathbf{0}, \mathbf{R}_{kl})$. \mathbf{R}_{kl} is the spatial correlation matrix that characterizes the channel's spatial properties, defined as $\mathbf{R}_{kl} = \mathbb{E}[\mathbf{h}_{kl} \mathbf{h}_{kl}^H]$. Large-scale fading coefficient, $\beta_{kl} = \text{tr}(\mathbf{R}_{kl})/N_a$, accounts for geometric path loss and shadowing. The generation of the channel realization is based on $\mathbf{h}_{kl} = \mathbf{R}_{kl}^{1/2} \mathbf{h}'_{kl}$, where \mathbf{h}'_{kl} denotes independent and identically distributed Rayleigh fading with zero-mean, unit-variance elements [28]. Similarly, we write $\mathbf{h}_{k0} \in \mathbb{C}^{N_b}$ to denote the channel between the cBS and user k , $\forall k \in \mathbb{K}$. It follows the distribution $\mathcal{CN}(\mathbf{0}, \mathbf{R}_{k0})$, where \mathbf{R}_{k0} is the spatial correlation matrix, and its corresponding large-scale fading coefficient equals $\beta_{k0} = \text{tr}(\mathbf{R}_{k0})/N_b$. Since spatial correlation matrix does not change rapidly over time or frequency, the system can measure it on a long-term basis and distributes it periodically. Thus, it is reasonable to assume that all nodes have perfect knowledge of this information.

To avoid the prohibitive overhead of downlink pilots, which scales with the number of service antennas, time-division duplexing (TDD) is employed in massive MIMO to separate the downlink and uplink transmission. Thus, each coherent block is split into three phases: uplink training, uplink data transmission, and downlink data transmission. In the downlink, all eAPs and cBS transmit data symbols over the same time-frequency resource, while all UEs simultaneously send their signals in the uplink at another instant.

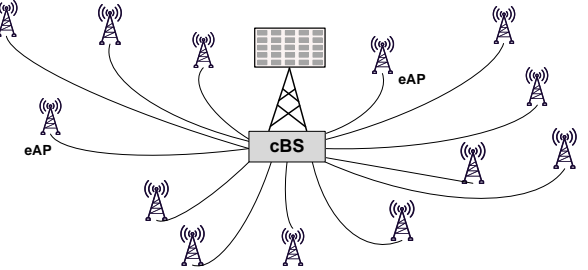
III. UPLINK TRAINING

Assume pilot sequences span τ_p symbols, allowing for a maximum of τ_p orthogonal sequences, which are collectively represented as $\boldsymbol{\Omega} = [\boldsymbol{\omega}_1, \dots, \boldsymbol{\omega}_{\tau_p}] \in \mathbb{C}^{\tau_p \times \tau_p}$. These

¹Most prior works on CF have simplified analyses by assuming either single-antenna APs or multi-antenna APs with independent channels among an AP's co-located antennas. However, in practical scenarios, closely spaced antennas at a multi-antenna AP exhibit correlated channel responses. Thus, it is essential to consider channel correlations for precious performance evaluation and system design.



(a) CF: a large number of distributed APs cooperatively cover an area, coordinated by a CPU through a large-scale fronthaul network.



(b) HCF: a cBS equipped with a massive antenna array, aided by some distributed eAPs, which are connected to the cBS.

Fig. 1. A comparative illustration of cell-free and hierarchical cell-free massive MIMO networks.

sequences have unit-magnitude elements for a constant power level, implying that $\boldsymbol{\Omega} \boldsymbol{\Omega}^H = \tau_p \mathbf{I}_{\tau_p}$. During the uplink training phase, each UE transmits a pilot sequence. Denoting the pilot sequence of UE k by \mathbf{i}_k , we have $\exists! x \in \{1, \dots, \tau_p\}$ ($\mathbf{i}_k = \boldsymbol{\omega}_x$), where $\exists!$ stands for unique existential quantification.

1) *eAP-UE Channel Estimation*: When the UEs simultaneously transmit their pilot sequences, the received pilot signal at a typical eAP l is given by

$$\boldsymbol{\Psi}_l = \sqrt{p_u} \sum_{k \in \mathbb{K}} \mathbf{h}_{kl} \mathbf{i}_k^T + \mathbf{Z}_l, \quad (1)$$

where p_u is UE's transmit power constraint and $\mathbf{Z}_l \in \mathbb{C}^{N_a \times \tau_p}$ represents additive noise with independent entries following the distribution of $\mathcal{CN}(0, \sigma_z^2)$, where σ_z^2 is the noise power. From the scalability perspective, some UEs need to share the same sequence if $\tau_p < K$, when the system simultaneously serves a lot of active users. This leads to pilot contamination [29]. We use \mathcal{P}_k to denote the set of indices for the users, including user k itself, that utilize the same sequence of \mathbf{i}_k .

To estimate \mathbf{h}_{kl} , correlate $\boldsymbol{\Psi}_l$ with the known pilot sequence \mathbf{i}_k , resulting in²

$$\begin{aligned} \boldsymbol{\psi}_{kl} &= \boldsymbol{\Psi}_l \mathbf{i}_k^* = \sqrt{p_u} \sum_{k' \in \mathbb{K}} \mathbf{h}_{k'l} \mathbf{i}_{k'}^T \mathbf{i}_k^* + \mathbf{Z}_l \mathbf{i}_k^* \\ &= \sqrt{p_u} \tau_p \mathbf{h}_{kl} + \sqrt{p_u} \tau_p \sum_{k' \in \mathcal{P}_k \setminus \{k\}} \mathbf{h}_{k'l} + \mathbf{Z}_l \mathbf{i}_k^*, \end{aligned} \quad (2)$$

as $\mathbf{i}_{k'}^T \mathbf{i}_k^* = 0$, when $k' \notin \mathcal{P}_k$. Conducting channel estimation with linear MMSE [30], the estimate of \mathbf{h}_{kl} is obtained by

$$\hat{\mathbf{h}}_{kl} = \mathbb{E} \left[\mathbf{h}_{kl} \boldsymbol{\psi}_{kl}^H \right] \left(\mathbb{E} \left[\boldsymbol{\psi}_{kl} \boldsymbol{\psi}_{kl}^H \right] \right)^{-1} \boldsymbol{\psi}_{kl}. \quad (3)$$

²In this paper, a *general* user is denoted by k' , while a *particular* user, which is under analysis and discussion, is represented by k .

In our case,

$$\begin{aligned}\mathbb{E} [\mathbf{h}_{kl} \boldsymbol{\psi}_{kl}^H] &= \sqrt{p_u} \tau_p \mathbb{E} [\mathbf{h}_{kl} \mathbf{h}_{kl}^H] \\ &+ \sqrt{p_u} \tau_p \sum_{k' \in \mathcal{P}_k \setminus \{k\}} \mathbb{E} [\mathbf{h}_{kl} \mathbf{h}_{k'l}^H] + \mathbb{E} [\mathbf{h}_{kl} \mathbf{Z}_l \mathbf{i}_k^*] \\ &= \sqrt{p_u} \tau_p \mathbf{R}_{kl},\end{aligned}\quad (4)$$

and

$$\begin{aligned}\mathbb{E} [\boldsymbol{\psi}_{kl} \boldsymbol{\psi}_{kl}^H] &= p_u \tau_p^2 \sum_{k' \in \mathcal{P}_k} \mathbb{E} [\mathbf{h}_{k'l} \mathbf{h}_{k'l}^H] + \mathbb{E} [\mathbf{Z}_l \mathbf{i}_k \mathbf{i}_k^H \mathbf{Z}_l^H] \\ &= \tau_p \left(p_u \tau_p \sum_{k' \in \mathcal{P}_k} \mathbf{R}_{k'l} + \sigma_z^2 \mathbf{I}_{N_a} \right).\end{aligned}\quad (5)$$

Hence, (3) can be rewritten as

$$\hat{\mathbf{h}}_{kl} = \sqrt{p_u} \mathbf{R}_{kl} \boldsymbol{\Gamma}_{kl}^{-1} \boldsymbol{\psi}_{kl}, \quad (6)$$

where

$$\boldsymbol{\Gamma}_{kl} = p_u \tau_p \sum_{k' \in \mathcal{P}_k} \mathbf{R}_{k'l} + \sigma_z^2 \mathbf{I}_{N_a}. \quad (7)$$

The correlation matrix of $\hat{\mathbf{h}}_{kl}$ is computed by

$$\begin{aligned}\mathbb{E} [\hat{\mathbf{h}}_{kl} \hat{\mathbf{h}}_{kl}^H] &= \mathbb{E} [\mathbf{h}_{kl} \boldsymbol{\psi}_{kl}^H] \left(\mathbb{E} [\boldsymbol{\psi}_{kl} \boldsymbol{\psi}_{kl}^H] \right)^{-1} \mathbb{E} [\boldsymbol{\psi}_{kl} \mathbf{h}_{kl}^H] \\ &= p_u \tau_p \mathbf{R}_{kl} \boldsymbol{\Gamma}_{kl}^{-1} \mathbf{R}_{kl},\end{aligned}\quad (8)$$

implying that $\hat{\mathbf{h}}_{kl}$ follows a complex Gaussian distribution:

$$\hat{\mathbf{h}}_{kl} \sim \mathcal{CN}(\mathbf{0}, p_u \tau_p \mathbf{R}_{kl} \boldsymbol{\Gamma}_{kl}^{-1} \mathbf{R}_{kl}). \quad (9)$$

The estimation error, defined as $\tilde{\mathbf{h}}_{kl} = \mathbf{h}_{kl} - \hat{\mathbf{h}}_{kl}$, arises due to additive noise and pilot contamination, following $\mathcal{CN}(\mathbf{0}, \boldsymbol{\Theta}_{kl})$, where its correlation matrix is given by

$$\boldsymbol{\Theta}_{kl} = \mathbb{E} [\tilde{\mathbf{h}}_{kl} \tilde{\mathbf{h}}_{kl}^H] = \mathbf{R}_{kl} - p_u \tau_p \mathbf{R}_{kl} \boldsymbol{\Gamma}_{kl}^{-1} \mathbf{R}_{kl}. \quad (10)$$

Based on the system implementation, channel estimation can be conducted distributedly at each eAP or centrally at the cBS. For eAP l , transmitting $\boldsymbol{\Psi}_l$ over the fronthaul requires $N_a \times \tau_p$ complex scalars per coherent block. It is more efficient than performing *local* channel estimation and then sending the channel estimates $\{\mathbf{h}_{kl}\}_{k \in \mathbb{K}}$, which require $N_a \times K$ complex scalars, as $K > \tau_p$ in most scenarios. Hence, we assume the use of centralized estimation in our article.

2) *cBS-UE Channel Estimation*: Likewise, the cBS sees

$$\boldsymbol{\Psi}_0 = \sqrt{p_u} \sum_{k \in \mathbb{K}} \mathbf{h}_{k0} \mathbf{i}_k^T + \mathbf{Z}_0, \quad (11)$$

where $\mathbf{Z}_0 \in \mathbb{C}^{N_b \times \tau_p}$ represents the receiver noise at the cBS. Its channel estimation process mirrors that of the eAPs. Consequently, we obtain the MMSE estimate

$$\hat{\mathbf{h}}_{k0} \sim \mathcal{CN}(\mathbf{0}, p_u \tau_p \mathbf{R}_{k0} \boldsymbol{\Gamma}_{k0}^{-1} \mathbf{R}_{k0}), \quad (12)$$

where $\boldsymbol{\Gamma}_{k0} = p_u \tau_p \sum_{k' \in \mathcal{P}_k} \mathbf{R}_{k'0} + \sigma_z^2 \mathbf{I}_{N_b}$. The estimation error follows the distribution of $\tilde{\mathbf{h}}_{k0} \sim \mathcal{CN}(\mathbf{0}, \boldsymbol{\Theta}_{k0})$ with

$$\boldsymbol{\Theta}_{k0} = \mathbb{E} [\tilde{\mathbf{h}}_{k0} \tilde{\mathbf{h}}_{k0}^H] = \mathbf{R}_{k0} - p_u \tau_p \mathbf{R}_{k0} \boldsymbol{\Gamma}_{k0}^{-1} \mathbf{R}_{k0}. \quad (13)$$

IV. UPLINK DATA TRANSMISSION

In the uplink, all UEs simultaneously transmit their information-bearing symbols, where UE k transmits x_k with a power coefficient $0 \leq \eta_k \leq 1$. These symbols are zero-mean, have unit variance, and are mutually uncorrelated. That is, the covariance matrix of $\mathbf{x} = [x_1, \dots, x_K]^T$ satisfies $\mathbb{E}[\mathbf{x} \mathbf{x}^H] = \mathbf{I}_K$.

A. Signal Detection for HCF Massive MIMO

During each channel use, eAP l receives

$$\mathbf{y}_l = \sqrt{p_u} \sum_{k \in \mathbb{K}} \sqrt{\eta_k} \mathbf{h}_{kl} x_k + \mathbf{z}_l, \quad (14)$$

where the receiver noise $\mathbf{z}_l \sim \mathcal{CN}(\mathbf{0}, \sigma_z^2 \mathbf{I}_{N_a})$. Meanwhile, the cBS observes

$$\mathbf{y}_0 = \sqrt{p_u} \sum_{k \in \mathbb{K}} \sqrt{\eta_k} \mathbf{h}_{k0} x_k + \mathbf{z}_0$$

with $\mathbf{z}_0 \sim \mathcal{CN}(\mathbf{0}, \sigma_z^2 \mathbf{I}_{N_b})$.

For ease of exposition, we employ the matched filtering (MF) detection method, also referred to as maximum-ratio combining [5]. Additionally, we assume centralized processing [12], where eAP l transmits \mathbf{y}_l to the cBS via the fronthaul network. To recover x_k , the cBS correlates \mathbf{y}_0 with the MF combining vector that equals to $\hat{\mathbf{h}}_{k0}$, and multiplies \mathbf{y}_l by $\hat{\mathbf{h}}_{kl}^H$ for all $l \in \mathbb{L}$. This produces a soft estimate of x_k as

$$\begin{aligned}\hat{x}_k &= \frac{1}{\sqrt{p_u}} \left(\hat{\mathbf{h}}_{k0}^H \mathbf{y}_0 + \sum_{l \in \mathbb{L}} \hat{\mathbf{h}}_{kl}^H \mathbf{y}_l \right) \\ &= \hat{\mathbf{h}}_{k0}^H \left(\sum_{k' \in \mathbb{K}} \sqrt{\eta_{k'}} \mathbf{h}_{k'0} x_{k'} + \frac{1}{\sqrt{p_u}} \mathbf{z}_0 \right) \\ &+ \sum_{l \in \mathbb{L}} \hat{\mathbf{h}}_{kl}^H \left(\sum_{k' \in \mathbb{K}} \sqrt{\eta_{k'}} \mathbf{h}_{k'l} x_{k'} + \frac{1}{\sqrt{p_u}} \mathbf{z}_l \right).\end{aligned}\quad (15)$$

Proposition 1. *The achievable SE for user k in the uplink of HCF massive MIMO systems is expressed as*

$$R_k^{hcf} = \left(1 - \frac{\tau_p}{\tau_u} \right) \mathbb{E} \left[\log_2 \left(1 + \gamma_k^{hcf} \right) \right], \quad (16)$$

where the pre-log factor $1 - \tau_p/\tau_u$ accounts for the overhead of uplink pilots, and the instantaneous effective signal-to-interference-plus-noise ratio (SINR) is given by

$$\gamma_k^{hcf} = \frac{\eta_k \left(\|\hat{\mathbf{h}}_{k0}\|^2 + \sum_{l \in \mathbb{L}} \|\hat{\mathbf{h}}_{kl}\|^2 \right)^2}{\left\{ \begin{array}{l} \sum_{k' \in \mathbb{K}} \eta_{k'} \left(\hat{\mathbf{h}}_{k0}^H \boldsymbol{\Theta}_{k'0} \hat{\mathbf{h}}_{k0} + \sum_{l \in \mathbb{L}} \hat{\mathbf{h}}_{kl}^H \boldsymbol{\Theta}_{k'l} \hat{\mathbf{h}}_{kl} \right) \\ + \sum_{k' \in \mathbb{K} \setminus \{k\}} \eta_{k'} \left| \hat{\mathbf{h}}_{k0}^H \hat{\mathbf{h}}_{k'0} + \sum_{l \in \mathbb{L}} \hat{\mathbf{h}}_{kl}^H \hat{\mathbf{h}}_{k'l} \right|^2 \\ + \frac{\sigma_z^2}{p_u} \left(\|\hat{\mathbf{h}}_{k0}\|^2 + \sum_{l \in \mathbb{L}} \|\hat{\mathbf{h}}_{kl}\|^2 \right) \end{array} \right\}}. \quad (17)$$

Proof: To facilitate the derivation, (15) is rewritten as

$$\begin{aligned} \hat{x}_k &= \underbrace{\sqrt{\eta_k} \left[\hat{\mathbf{h}}_{k0}^H \hat{\mathbf{h}}_{k0} + \sum_{l \in \mathbb{L}} \hat{\mathbf{h}}_{kl}^H \hat{\mathbf{h}}_{kl} \right] x_k}_{\mathcal{S}_0: \text{desired signal}} \\ &+ \underbrace{\sum_{k' \in \mathbb{K}} \sqrt{\eta_{k'}} \left[\hat{\mathbf{h}}_{k0}^H \tilde{\mathbf{h}}_{k'0} + \sum_{l \in \mathbb{L}} \hat{\mathbf{h}}_{kl}^H \tilde{\mathbf{h}}_{k'l} \right] x_{k'}}_{\mathcal{I}_1: \text{channel estimation error}} \\ &+ \underbrace{\sum_{k' \in \mathbb{K} \setminus \{k\}} \sqrt{\eta_{k'}} \left[\hat{\mathbf{h}}_{k0}^H \hat{\mathbf{h}}_{k'0} + \sum_{l \in \mathbb{L}} \hat{\mathbf{h}}_{kl}^H \hat{\mathbf{h}}_{k'l} \right] x_{k'}}_{\mathcal{I}_2: \text{inter-user interference}} \\ &+ \underbrace{\frac{1}{\sqrt{p_u}} \left(\hat{\mathbf{h}}_{k0}^H \mathbf{z}_0 + \sum_{l \in \mathbb{L}} \hat{\mathbf{h}}_{kl}^H \mathbf{z}_l \right)}_{\mathcal{I}_3: \text{colored noise}}. \end{aligned} \quad (18)$$

Due to the independence among data symbols, channel estimates, and estimation errors, the interference terms \mathcal{I}_1 , \mathcal{I}_2 , and \mathcal{I}_3 exhibit mutual uncorrelation. As stated in [31], the worst-case noise for mutual information corresponds to Gaussian additive noise with a variance equal to the sum of the variances of \mathcal{I}_1 , \mathcal{I}_2 , and \mathcal{I}_3 . Thus, the effective SINR is given by

$$\gamma_k^{hcf} = \frac{|\mathcal{S}_0|^2}{\mathbb{E}[|\mathcal{I}_1 + \mathcal{I}_2 + \mathcal{I}_3|^2]} = \frac{|\mathcal{S}_0|^2}{\mathbb{E}[|\mathcal{I}_1|^2] + \mathbb{E}[|\mathcal{I}_2|^2] + \mathbb{E}[|\mathcal{I}_3|^2]}, \quad (19)$$

where the power gain of the desired signal equals

$$\begin{aligned} |\mathcal{S}_0|^2 &= \eta_k \left| \hat{\mathbf{h}}_{k0}^H \hat{\mathbf{h}}_{k0} + \sum_{l \in \mathbb{L}} \hat{\mathbf{h}}_{kl}^H \hat{\mathbf{h}}_{kl} \right|^2 \\ &= \eta_k \left(\|\hat{\mathbf{h}}_{k0}\|^2 + \sum_{l \in \mathbb{L}} \|\hat{\mathbf{h}}_{kl}\|^2 \right)^2. \end{aligned} \quad (20)$$

Since $\{\hat{\mathbf{h}}_{k0}\}_{k \in \mathbb{K}}$ and $\{\hat{\mathbf{h}}_{kl}\}_{k \in \mathbb{K}, l \in \mathbb{L}}$ are *deterministic* for the cBS, see [30], the conditional variance of \mathcal{I}_1 is derived as

$$\begin{aligned} \mathbb{E}[|\mathcal{I}_1|^2] &\stackrel{(a)}{=} \sum_{k' \in \mathbb{K}} \eta_{k'} \mathbb{E} \left[\left| \hat{\mathbf{h}}_{k0}^H \tilde{\mathbf{h}}_{k'0} + \sum_{l \in \mathbb{L}} \hat{\mathbf{h}}_{kl}^H \tilde{\mathbf{h}}_{k'l} \right|^2 \right] \quad (21) \\ &\stackrel{(b)}{=} \sum_{k' \in \mathbb{K}} \eta_{k'} \left(\mathbb{E}[|\hat{\mathbf{h}}_{k0}^H \tilde{\mathbf{h}}_{k'0}|^2] + \sum_{l \in \mathbb{L}} \mathbb{E}[|\hat{\mathbf{h}}_{kl}^H \tilde{\mathbf{h}}_{k'l}|^2] \right) \\ &\stackrel{(c)}{=} \sum_{k' \in \mathbb{K}} \eta_{k'} \left(\hat{\mathbf{h}}_{k0}^H \mathbb{E} \left[\tilde{\mathbf{h}}_{k'0} \tilde{\mathbf{h}}_{k'0}^H \right] \hat{\mathbf{h}}_{k0} \right. \\ &\quad \left. + \sum_{l \in \mathbb{L}} \hat{\mathbf{h}}_{kl}^H \mathbb{E} \left[\tilde{\mathbf{h}}_{k'l} \tilde{\mathbf{h}}_{k'l}^H \right] \hat{\mathbf{h}}_{kl} \right) \\ &= \sum_{k' \in \mathbb{K}} \eta_{k'} \left(\hat{\mathbf{h}}_{k0}^H \Theta_{k'0} \hat{\mathbf{h}}_{k0} + \sum_{l \in \mathbb{L}} \hat{\mathbf{h}}_{kl}^H \Theta_{k'l} \hat{\mathbf{h}}_{kl} \right), \end{aligned}$$

where the derivations (a) follows from the orthonormality of symbols, i.e., $\mathbb{E}[x_{k'}^* x_k] = 0$ for $k' \neq k$, and $\mathbb{E}[|x_k|^2] = 1$ for any k ; (b) uses the fact that the variance of a sum of independent random variables equals the sum of their variances; and (c) is based on the independence between channel estimates and their estimation errors.

Similarly, the variance of \mathcal{I}_2 is computed as

$$\begin{aligned} \mathbb{E}[|\mathcal{I}_2|^2] &= \sum_{k' \in \mathbb{K} \setminus \{k\}} \eta_{k'} \mathbb{E} \left[\left| \hat{\mathbf{h}}_{k0}^H \hat{\mathbf{h}}_{k'0} + \sum_{l \in \mathbb{L}} \hat{\mathbf{h}}_{kl}^H \hat{\mathbf{h}}_{k'l} \right|^2 \right] \\ &= \sum_{k' \in \mathbb{K} \setminus \{k\}} \eta_{k'} \left| \hat{\mathbf{h}}_{k0}^H \hat{\mathbf{h}}_{k'0} + \sum_{l \in \mathbb{L}} \hat{\mathbf{h}}_{kl}^H \hat{\mathbf{h}}_{k'l} \right|^2, \end{aligned} \quad (22)$$

due to the deterministic nature of the channel estimates. The variance of \mathcal{I}_3 equals to

$$\begin{aligned} \mathbb{E}[\mathcal{I}_3^2] &= \frac{1}{p_u} \mathbb{E} \left[\left| \hat{\mathbf{h}}_{k0}^H \mathbf{z}_0 + \sum_{l \in \mathbb{L}} \hat{\mathbf{h}}_{kl}^H \mathbf{z}_l \right|^2 \right] \quad (23) \\ &= \frac{1}{p_u} \mathbb{E} \left[\left| \hat{\mathbf{h}}_{k0}^H \mathbf{z}_0 \right|^2 \right] + \sum_{l \in \mathbb{L}} \mathbb{E} \left[\left| \hat{\mathbf{h}}_{kl}^H \mathbf{z}_l \right|^2 \right] \\ &= \frac{1}{p_u} \left(\hat{\mathbf{h}}_{k0}^H \mathbb{E}[\mathbf{z}_0 \mathbf{z}_0^H] \hat{\mathbf{h}}_{k0} + \sum_{l \in \mathbb{L}} \hat{\mathbf{h}}_{kl}^H \mathbb{E}[\mathbf{z}_l \mathbf{z}_l^H] \hat{\mathbf{h}}_{kl} \right) \\ &= \frac{\sigma_z^2}{p_u} \left(\hat{\mathbf{h}}_{k0}^H \mathbf{I}_{N_b} \hat{\mathbf{h}}_{k0} + \sum_{l \in \mathbb{L}} \hat{\mathbf{h}}_{kl}^H \mathbf{I}_{N_a} \hat{\mathbf{h}}_{kl} \right) \\ &= \frac{\sigma_z^2}{p_u} \left(\|\hat{\mathbf{h}}_{k0}\|^2 + \sum_{l \in \mathbb{L}} \|\hat{\mathbf{h}}_{kl}\|^2 \right). \end{aligned}$$

Substituting these variances into (19) yields (17). ■

Algorithm 1: Uplink HCF Max-Min Power Control

Input: $\{\hat{\mathbf{h}}_{k0}, \hat{\mathbf{h}}_{kl}, \Theta_{k0}, \Theta_{kl}\}_{k \in \mathbb{K}, l \in \mathbb{L}}, p_u, \sigma_z^2, \epsilon$;
Output: Optimal power coefficients $\{\eta_k^*\}_{k \in \mathbb{K}}$

Initialization:
 $t \leftarrow 0$
 $\gamma_{\text{low}}^{(0)} \leftarrow 0, \quad \gamma_{\text{high}}^{(0)} \leftarrow \max \left\{ \frac{(\|\hat{\mathbf{h}}_{k0}\|^2 + \sum_{l \in \mathbb{L}} \|\hat{\mathbf{h}}_{kl}\|^2) p_u}{\sigma_z^2} \right\}$

while $\gamma_{\text{high}}^{(t)} - \gamma_{\text{low}}^{(t)} > \epsilon$ **do**
 $\gamma_t \leftarrow \frac{1}{2}(\gamma_{\text{low}}^{(t)} + \gamma_{\text{high}}^{(t)})$

Convex Feasibility Check:

Find $\{\eta_k\}_{k \in \mathbb{K}}$
s.t. $\gamma_k^{hcf} \geq \gamma_t, \forall k \in \mathbb{K}$
 $0 \leq \eta_k \leq 1, \forall k \in \mathbb{K}$

if feasible then
 $\gamma_{\text{low}}^{(t+1)} \leftarrow \gamma_t, \quad \gamma_{\text{high}}^{(t+1)} \leftarrow \gamma_{\text{high}}^{(t)}$
 $\eta_k^* \leftarrow \eta_k$

end

else
 $\gamma_{\text{low}}^{(t+1)} \leftarrow \gamma_{\text{low}}^{(t)}, \quad \gamma_{\text{high}}^{(t+1)} \leftarrow \gamma_t$

end
 $t \leftarrow t + 1$

end
return $\{\eta_k^*\}_{k \in \mathbb{K}}$

B. Max-Min Uplink Power Optimization

Max-min power control has proven highly effective in enhancing fairness for CF systems [5], [32]. Building on this insight, we design a HCF max-min fairness algorithm to dynamically adjust UE's transmit power in the uplink. The optimization formula can be represented as

$$\begin{aligned} \max_{\{\eta_k\}_{k \in \mathbb{K}}} \min_k \quad & \gamma_k^{hcf} \\ \text{s.t.} \quad & 0 \leq \eta_k \leq 1, \quad \forall k \in \mathbb{K} \end{aligned} \quad (24)$$

Introducing a slack variable γ_t , which represents the minimum SINR across users, the problem is reformulated as

$$\begin{aligned} \max_{\{\eta_k\}_{k \in \mathbb{K}}, \gamma_t} \quad & \gamma_t \\ \text{s.t.} \quad & \gamma_k^{hcf} \geq \gamma_t, \quad \forall k \\ & 0 \leq \eta_k \leq 1, \quad \forall k \in \mathbb{K}. \end{aligned} \quad (25)$$

Since γ_k^{hcf} is quasiconcave with respect to $\{\eta_k\}_{k \in \mathbb{K}}$, the constraint set $\gamma_k^{hcf} \geq \gamma_t$ is convex. Therefore, for a fixed γ_t , the constraint domain in (25) is convex, making it straightforward to determine whether a given γ_t is feasible. Consequently, the bisection method is applied: first, we select an interval $(\gamma_{low}, \gamma_{high})$ that contains the optimal value γ_t^* . Then, we check the feasibility of the midpoint $\gamma_t = \frac{\gamma_{low} + \gamma_{high}}{2}$. If γ_t is feasible, the search interval is updated to $(\gamma_t, \gamma_{high})$; otherwise, it is updated to (γ_{low}, γ_t) . This process repeats until the search interval is sufficiently small, less than a tolerance $\epsilon > 0$, as depicted in Algorithm 1.

C. Cellular Massive MIMO

To facilitate comparison, we analyze cellular systems, deriving its closed-form SE expression under spatially correlated channels and pilot contamination. In the uplink of a cellular system, the BS observes

$$\mathbf{y}_b = \sqrt{p_u} \sum_{k \in \mathbb{K}} \sqrt{\eta_k} \mathbf{g}_k x_k + \mathbf{z}_b, \quad (26)$$

where $\mathbf{g}_k \in \mathbb{C}^M$ represents the channel vector between the BS antennas and user k , and the receiver noise $\mathbf{z}_b \sim \mathcal{CN}(\mathbf{0}, \sigma_z^2 \mathbf{I}_M)$. Let $\hat{\mathbf{g}}_k$ be the MMSE estimate of \mathbf{g}_k , and the estimation error $\tilde{\mathbf{g}}_k = \mathbf{g}_k - \hat{\mathbf{g}}_k$ follows a complex Gaussian distribution, $\tilde{\mathbf{g}}_k \sim \mathcal{CN}(\mathbf{0}, \Theta_k)$. The covariance matrix Θ_k is

$$\Theta_k = \mathbb{E}[\tilde{\mathbf{g}}_k \tilde{\mathbf{g}}_k^H] = \mathbf{R}_k - p_u \tau_p \mathbf{R}_k \Gamma_k^{-1} \mathbf{R}_k, \quad (27)$$

where $\mathbf{R}_k = \mathbb{E}[\mathbf{g}_k \mathbf{g}_k^H]$ is the spatial correlation matrix, and $\Gamma_k = p_u \tau_p \sum_{k' \in \mathcal{P}_k} \mathbf{R}_{k'} + \sigma_z^2 \mathbf{I}_M$. The BS correlates \mathbf{y}_b with $\hat{\mathbf{g}}_k$, to generate a soft estimate of x_k , as follows:

$$\begin{aligned} \hat{x}_k &= \frac{1}{\sqrt{p_u}} \hat{\mathbf{g}}_k^H \mathbf{y}_b \\ &= \sqrt{\eta_k} \hat{\mathbf{g}}_k^H (\hat{\mathbf{g}}_k + \tilde{\mathbf{g}}_k) x_k + \sum_{k' \in \mathbb{K} \setminus \{k\}} \sqrt{\eta_{k'}} \hat{\mathbf{g}}_k^H \mathbf{g}_{k'} x_{k'} + \frac{\hat{\mathbf{g}}_k^H \mathbf{z}_b}{\sqrt{p_u}}. \end{aligned} \quad (28)$$

Proposition 2. The achievable SE for user k in the uplink of a cellular system, considering correlated channels and pilot contamination, is expressed as $R_k^c = (1 - \frac{\tau_p}{\tau_u}) \mathbb{E}[\log_2(1 + \gamma_k^c)]$, where the instantaneous effective SINR is

$$\gamma_k^c = \frac{\eta_k \|\hat{\mathbf{g}}_k\|^4}{\hat{\mathbf{g}}_k^H \left(\sum_{k' \in \mathbb{K} \setminus \{k\}} \eta_{k'} \hat{\mathbf{g}}_{k'} \hat{\mathbf{g}}_{k'}^H + \sum_{k' \in \mathbb{K}} \eta_{k'} \Theta_{k'} + \frac{\sigma_z^2}{p_u} \mathbf{I}_M \right) \hat{\mathbf{g}}_k}. \quad (29)$$

D. Cell-Free Massive MIMO

We derive closed-form SE expression for CF systems under spatially correlated channels and pilot contamination. This goes beyond previous works, which were primarily limited to

single-antenna APs or independent channels. In a CF system with $A = \frac{M}{N_a}$ distributed APs, each equipped with N_a antennas, the received signal at AP a , where $a \in \mathbb{A} = \{1, \dots, A\}$, is expressed by

$$\mathbf{y}_a = \sqrt{p_u} \sum_{k \in \mathbb{K}} \sqrt{\eta_k} \mathbf{g}_{ka} x_k + \mathbf{z}_a. \quad (30)$$

Here, the receiver noise $\mathbf{z}_a \sim \mathcal{CN}(\mathbf{0}, \sigma_z^2 \mathbf{I}_{N_a})$, and $\mathbf{g}_{ka} \in \mathbb{C}^{N_a}$ denotes the channel vector between AP a and user k . Similarly, the MMSE estimate of \mathbf{g}_{ka} is denoted as $\hat{\mathbf{g}}_{ka}$, while the estimation error $\tilde{\mathbf{g}}_{ka} = \mathbf{g}_{ka} - \hat{\mathbf{g}}_{ka}$ follows $\mathcal{CN}(\mathbf{0}, \Theta_{ka})$. Its covariance matrix $\Theta_{ka} = \mathbf{R}_{ka} - p_u \tau_p \mathbf{R}_{ka} \Gamma_{ka}^{-1} \mathbf{R}_{ka}$, with $\mathbf{R}_{ka} = \mathbb{E}[\mathbf{g}_{ka} \mathbf{g}_{ka}^H]$ and $\Gamma_{ka} = p_u \tau_p \sum_{k' \in \mathcal{P}_k} \mathbf{R}_{k'a} + \sigma_z^2 \mathbf{I}_{N_a}$. For a fair comparison, we consider that the CPU performs centralized MF combining based on the received signals forwarded by the APs, resulting in a soft estimate of

$$\begin{aligned} \hat{x}_k &= \frac{1}{\sqrt{p_u}} \sum_{a \in \mathbb{A}} \hat{\mathbf{g}}_{ka}^H \mathbf{y}_a \\ &= \sum_{a \in \mathbb{A}} \hat{\mathbf{g}}_{ka}^H \left(\sum_{k' \in \mathbb{K}} \sqrt{\eta_{k'}} \mathbf{g}_{k'a} x_{k'} + \frac{1}{\sqrt{p_u}} \mathbf{z}_a \right) \\ &= \sqrt{\eta_k} \sum_{a \in \mathbb{A}} \hat{\mathbf{g}}_{ka}^H \hat{\mathbf{g}}_{ka} x_k + \sum_{k' \in \mathbb{K}} \sqrt{\eta_{k'}} \sum_{a \in \mathbb{A}} \hat{\mathbf{g}}_{ka}^H \tilde{\mathbf{g}}_{k'a} x_{k'} \\ &\quad + \sum_{k' \in \mathbb{K} \setminus \{k\}} \sqrt{\eta_{k'}} \sum_{a \in \mathbb{A}} \hat{\mathbf{g}}_{ka}^H \hat{\mathbf{g}}_{k'a} x_{k'} + \frac{1}{\sqrt{p_u}} \sum_{a \in \mathbb{A}} \hat{\mathbf{g}}_{ka}^H \mathbf{z}_a. \end{aligned} \quad (31)$$

Proposition 3. The achievable SE for user k in the uplink of a cell-free system, considering correlated channels and pilot contamination, is given by $R_k^{cf} = (1 - \frac{\tau_p}{\tau_u}) \mathbb{E}[\log_2(1 + \gamma_k^{cf})]$ with the effective SINR of

$$\gamma_k^{cf} = \frac{\eta_k (\sum_{a \in \mathbb{A}} \|\hat{\mathbf{g}}_{ka}\|^2)^2}{\left\{ \sum_{k' \in \mathbb{K}} \eta_{k'} \sum_{a \in \mathbb{A}} \hat{\mathbf{g}}_{ka}^H \Theta_{k'a} \hat{\mathbf{g}}_{ka} \right.} \\ \left. + \sum_{k' \in \mathbb{K} \setminus \{k\}} \eta_{k'} \left| \sum_{a \in \mathbb{A}} \hat{\mathbf{g}}_{ka}^H \hat{\mathbf{g}}_{k'a} \right|^2 + \frac{\sigma_z^2}{p_u} \sum_{a \in \mathbb{A}} \|\hat{\mathbf{g}}_{ka}\|^2 \right\}}. \quad (32)$$

V. DOWNLINK DATA TRANSMISSION

In the downlink, the information-bearing symbols intended for K users are modeled as zero-mean, unit-variance, and independent random variables. These symbols are collectively represented as $\mathbf{u} = [u_1, \dots, u_K]^T$, where $\mathbb{E}[\mathbf{u} \mathbf{u}^H] = \mathbf{I}_K$.

A. Linear Precoding for HCF Massive MIMO

Let $\mathbf{w}_{k0} \in \mathbb{C}^{N_b}$ denote the precoding vector for user k at the cBS. TDD channel reciprocity allows the cBS to utilize uplink channel estimates for downlink precoding [33]. To spatially multiplex symbols, the cBS employs conjugate beamforming (CBF) [5], i.e., $\mathbf{w}_{k0} = \hat{\mathbf{h}}_{k0}^* / \sqrt{\mathbb{E}[\|\hat{\mathbf{h}}_{k0}\|^2]}$, where the scaling is used to meet the normalization condition $\mathbb{E}[\|\mathbf{w}_{k0}\|^2] = 1$. Consequently, the cBS transmits

$$\mathbf{s}_0 = \sqrt{p_b} \sum_{k \in \mathbb{K}} \sqrt{\eta_{k0}} \mathbf{w}_{k0} u_k = \sqrt{p_b} \sum_{k \in \mathbb{K}} \frac{\sqrt{\eta_{k0}} \hat{\mathbf{h}}_{k0}^* u_k}{\sqrt{\mathbb{E}[\|\hat{\mathbf{h}}_{k0}\|^2]}}, \quad (34)$$

where η_{k0} indicates the power coefficient for user k at the cBS, and p_b denotes the maximum transmit power of the cBS.

$$\xi_k^{hcf} = \frac{\left(\sqrt{p_b \eta_{k0} p_u \tau_p \text{tr}(\mathbf{R}_{k0} \mathbf{\Gamma}_{k0}^{-1} \mathbf{R}_{k0})} + \sum_{l \in \mathbb{L}} \sqrt{p_a \eta_{kl} p_u \tau_p \text{tr}(\mathbf{R}_{kl} \mathbf{\Gamma}_{kl}^{-1} \mathbf{R}_{kl})} \right)^2}{\left\{ \begin{array}{l} p_b \sum_{k' \in \mathcal{P}_k \setminus \{k\}} \eta_{k'0} \frac{p_u \tau_p |\text{tr}(\mathbf{R}_{k0} \mathbf{\Gamma}_{k'0}^{-1} \mathbf{R}_{k'0})|^2}{\text{tr}(\mathbf{R}_{k'0} \mathbf{\Gamma}_{k'0}^{-1} \mathbf{R}_{k'0})} + p_b \sum_{k' \in \mathbb{K}} \eta_{k'0} \frac{\text{tr}(\mathbf{R}_{k0} \mathbf{R}_{k'0} \mathbf{\Gamma}_{k'0}^{-1} \mathbf{R}_{k'0})}{\text{tr}(\mathbf{R}_{k'0} \mathbf{\Gamma}_{k'0}^{-1} \mathbf{R}_{k'0})} \\ + p_a \sum_{k' \in \mathcal{P}_k \setminus \{k\}} \sum_{l \in \mathbb{L}} \eta_{k'l} \frac{p_u \tau_p |\text{tr}(\mathbf{R}_{kl} \mathbf{\Gamma}_{k'l}^{-1} \mathbf{R}_{k'l})|^2}{\text{tr}(\mathbf{R}_{k'l} \mathbf{\Gamma}_{k'l}^{-1} \mathbf{R}_{k'l})} + p_a \sum_{k' \in \mathbb{K}} \sum_{l \in \mathbb{L}} \eta_{k'l} \frac{\text{tr}(\mathbf{R}_{kl} \mathbf{R}_{k'l} \mathbf{\Gamma}_{k'l}^{-1} \mathbf{R}_{k'l})}{\text{tr}(\mathbf{R}_{k'l} \mathbf{\Gamma}_{k'l}^{-1} \mathbf{R}_{k'l})} + \sigma_z^2 \end{array} \right\}} \quad (33)$$

To meet the average power constraint, i.e., $\mathbb{E}[\|\mathbf{s}_0\|^2] \leq p_b$, the summation of coefficients must satisfy $\sum_{k \in \mathbb{K}} \eta_{k0} \leq 1$.

Similarly, let $\mathbf{w}_{kl} \in \mathbb{C}^{N_a}$ denote the precoding vector assigned to u_k at AP l . The cBS uses $\mathbf{w}_{kl} = \hat{\mathbf{h}}_{kl}^* / \sqrt{\mathbb{E}[\|\hat{\mathbf{h}}_{kl}\|^2]}$ to generate the transmit signal for eAP l , i.e.,

$$\mathbf{s}_l = \sqrt{p_a} \sum_{k \in \mathbb{K}} \sqrt{\eta_{kl}} \mathbf{w}_{kl} u_k = \sqrt{p_a} \sum_{k \in \mathbb{K}} \frac{\sqrt{\eta_{kl}} \hat{\mathbf{h}}_{kl}^* u_k}{\sqrt{\mathbb{E}[\|\hat{\mathbf{h}}_{kl}\|^2]}}, \quad (35)$$

where p_a stands for the maximum transmit power of eAPs, and η_{kl} represents the power coefficient for eAP l to user k , subject to the constraint $\sum_{k \in \mathbb{K}} \eta_{kl} \leq 1$ in order to satisfy $\mathbb{E}[\|\mathbf{s}_l\|^2] \leq p_a$. Sending $\{\mathbf{s}_l\}_{l \in \mathbb{L}}$ to the respective eAPs results in the transmission of $N_a \times L$ complex-valued scalars over the fronthaul network. With noise $n_k \sim \mathcal{CN}(0, \sigma_z^2)$, the observation at user k is given by $y_k = \mathbf{h}_{k0}^T \mathbf{s}_0 + \sum_{l \in \mathbb{L}} \mathbf{h}_{kl}^T \mathbf{s}_l + n_k$, which can be further expanded as

$$y_k = \sqrt{p_b} \sum_{k' \in \mathbb{K}} \sqrt{\eta_{k'0}} \mathbf{h}_{k0}^T \frac{\hat{\mathbf{h}}_{k'0}^*}{\sqrt{\mathbb{E}[\|\hat{\mathbf{h}}_{k'0}\|^2]}} u_{k'} + \sqrt{p_a} \sum_{k' \in \mathbb{K}} \sum_{l \in \mathbb{L}} \sqrt{\eta_{k'l}} \mathbf{h}_{kl}^T \frac{\hat{\mathbf{h}}_{k'l}^*}{\sqrt{\mathbb{E}[\|\hat{\mathbf{h}}_{k'l}\|^2]}} u_{k'} + n_k. \quad (36)$$

In massive MIMO, users typically do not know channel estimates due to the absence of downlink pilots [34], rendering coherent detection unfeasible. As a result, user k must rely on channel statistics $\mathbb{E}[\|\hat{\mathbf{h}}_{k0}\|^2]$ and $\{\mathbb{E}[\|\hat{\mathbf{h}}_{kl}\|^2]\}_{l \in \mathbb{L}}$ instead of channel estimates \mathbf{h}_{k0} and $\{\hat{\mathbf{h}}_{kl}\}_{l \in \mathbb{L}}$ to detect y_k . This introduces an additional performance loss, termed the *channel uncertainty error*, as marked by \mathcal{J}_1 in (37). To facilitate the derivation of the closed-form SE expression, (49)

is decomposed into

$$y_k = \underbrace{\left(\frac{\sqrt{p_b \eta_{k0}} \mathbb{E}[\hat{\mathbf{h}}_{k0}^T \hat{\mathbf{h}}_{k0}^*]}{\sqrt{\mathbb{E}[\|\hat{\mathbf{h}}_{k0}\|^2]}} + \sum_{l \in \mathbb{L}} \frac{\sqrt{p_a \eta_{kl}} \mathbb{E}[\hat{\mathbf{h}}_{kl}^T \hat{\mathbf{h}}_{kl}^*]}{\sqrt{\mathbb{E}[\|\hat{\mathbf{h}}_{kl}\|^2]}} \right) u_k}_{\mathcal{S}_1: \text{desired signal over channel statistics}} \\ + \underbrace{\left(\frac{\sqrt{p_b \eta_{k0}} (\mathbf{h}_{k0}^T \hat{\mathbf{h}}_{k0}^* - \mathbb{E}[\hat{\mathbf{h}}_{k0}^T \hat{\mathbf{h}}_{k0}^*])}{\sqrt{\mathbb{E}[\|\hat{\mathbf{h}}_{k0}\|^2]}} + \sqrt{p_a} \sum_{l \in \mathbb{L}} \frac{\sqrt{\eta_{kl}} (\mathbf{h}_{kl}^T \hat{\mathbf{h}}_{kl}^* - \mathbb{E}[\hat{\mathbf{h}}_{kl}^T \hat{\mathbf{h}}_{kl}^*])}{\sqrt{\mathbb{E}[\|\hat{\mathbf{h}}_{kl}\|^2]}} \right) u_k}_{\mathcal{J}_1: \text{channel uncertainty error}} \\ + \underbrace{\left(\sqrt{p_b} \sum_{k' \in \mathbb{K} \setminus \{k\}} \frac{\sqrt{\eta_{k'0}} \mathbf{h}_{k0}^T \hat{\mathbf{h}}_{k'0}^*}{\sqrt{\mathbb{E}[\|\hat{\mathbf{h}}_{k'0}\|^2]}} + \sqrt{p_a} \sum_{k' \in \mathbb{K} \setminus \{k\}} \sum_{l \in \mathbb{L}} \frac{\sqrt{\eta_{k'l}} \mathbf{h}_{kl}^T \hat{\mathbf{h}}_{k'l}^*}{\sqrt{\mathbb{E}[\|\hat{\mathbf{h}}_{k'l}\|^2]}} \right) u_{k'} + n_k}_{\mathcal{J}_2: \text{inter-user interference}} \quad (37)$$

Proposition 4. The achievable SE for user k in the downlink of HCF massive MIMO systems is expressed as $C_k^{hcf} = \mathbb{E}[\log_2(1 + \xi_k^{hcf})]$, where the effective SINR is given in (33).

Proof: The proof is detailed in Appendix (B). \blacksquare

B. Joint Max-Min Downlink Power Optimization

Given the downlink SINR expression in (33), we aim to design a max-min fairness algorithm for joint power control of the cBS and APs. The problem is formulated as [32]:

$$\max_{\{\eta_{k0}, \eta_{kl}\}_{k \in \mathbb{K}, l \in \mathbb{L}}} \min_{k \in \mathbb{K}} \xi_k^{hcf} \quad (38)$$

$$\text{s.t.} \quad \sum_{k \in \mathbb{K}} \eta_{k0} \leq 1, \quad \sum_{k \in \mathbb{K}} \eta_{kl} \leq 1, \quad \forall l \in \mathbb{L},$$

$$\eta_{k0} \geq 0, \quad \eta_{kl} \geq 0, \quad \forall k \in \mathbb{K}, l \in \mathbb{L}.$$

The numerator of ξ_k^{hcf} consists of a sum of square root terms, making it a concave function. To facilitate optimization, we introduce auxiliary variables $\nu_{k0} = \sqrt{\eta_{k0}}$ and $\nu_{kl} = \sqrt{\eta_{kl}}$, collectively denoted as $\boldsymbol{\nu} = \{\nu_{k0}, \nu_{kl}\}_{k \in \mathbb{K}, l \in \mathbb{L}}$.

Introducing a slack variable ξ_t to reformulate (38) into

$$\max_{\boldsymbol{\nu}, \xi_t} \xi_t \quad (39)$$

$$\text{s.t. } \begin{aligned} & \left(\nu_{k0} A_{k0} + \sum_{l \in \mathbb{L}} \nu_{kl} A_{kl} \right)^2 \geq \xi_t \mathcal{D}_k(\boldsymbol{\nu}), \\ & \sum_{k \in \mathbb{K}} \nu_{k0}^2 \leq 1, \quad \sum_{k \in \mathbb{K}} \nu_{kl}^2 \leq 1, \quad \forall l \in \mathbb{L}, \\ & \nu_{k0} \geq 0, \quad \nu_{kl} \geq 0, \quad \forall k \in \mathbb{K}, l \in \mathbb{L}. \end{aligned} \quad (\text{C1})$$

We define: $A_{k0} = \sqrt{p_b p_u \tau_p \text{tr}(\mathbf{R}_{k0} \boldsymbol{\Gamma}_{k0}^{-1} \mathbf{R}_{k0})}$ and $A_{kl} = \sqrt{p_a p_u \tau_p \text{tr}(\mathbf{R}_{kl} \boldsymbol{\Gamma}_{kl}^{-1} \mathbf{R}_{kl})}$, for ease of notation. The denominator of ξ_k^{hcf} is rewritten as

$$\begin{aligned} \mathcal{D}_k(\boldsymbol{\nu}) = & \sum_{k' \in \mathcal{P}_k \setminus \{k\}} \left(\nu_{k'0}^2 B_{k0,k'}^2 + \sum_{l \in \mathbb{L}} \nu_{k'l}^2 B_{kl,k'}^2 \right) \\ & + \sum_{k' \in \mathbb{K}} \left(\nu_{k'0}^2 C_{k0,k'}^2 + \sum_{l \in \mathbb{L}} \nu_{k'l}^2 C_{kl,k'}^2 \right) + \sigma_z^2, \end{aligned} \quad (40)$$

where

$$\begin{aligned} B_{k0,k'} &= \sqrt{\frac{p_b p_u \tau_p |\text{tr}(\mathbf{R}_{k0} \boldsymbol{\Gamma}_{k'0}^{-1} \mathbf{R}_{k'0})|^2}{\text{tr}(\mathbf{R}_{k'0} \boldsymbol{\Gamma}_{k'0}^{-1} \mathbf{R}_{k'0})}} \\ B_{kl,k'} &= \sqrt{\frac{p_a p_u \tau_p |\text{tr}(\mathbf{R}_{kl} \boldsymbol{\Gamma}_{k'l}^{-1} \mathbf{R}_{k'l})|^2}{\text{tr}(\mathbf{R}_{k'l} \boldsymbol{\Gamma}_{k'l}^{-1} \mathbf{R}_{k'l})}} \end{aligned} \quad (41)$$

and

$$\begin{aligned} C_{k0,k'} &= \sqrt{\frac{p_b \text{tr}(\mathbf{R}_{k0} \mathbf{R}_{k'0} \boldsymbol{\Gamma}_{k'0}^{-1} \mathbf{R}_{k'0})}{\text{tr}(\mathbf{R}_{k'0} \boldsymbol{\Gamma}_{k'0}^{-1} \mathbf{R}_{k'0})}} \\ C_{kl,k'} &= \sqrt{\frac{p_a \text{tr}(\mathbf{R}_{kl} \mathbf{R}_{k'l} \boldsymbol{\Gamma}_{k'l}^{-1} \mathbf{R}_{k'l})}{\text{tr}(\mathbf{R}_{k'l} \boldsymbol{\Gamma}_{k'l}^{-1} \mathbf{R}_{k'l})}}. \end{aligned} \quad (42)$$

The left-hand side of constraint (C1) in (39) is a convex quadratic function, while the right-hand side is convex in $\boldsymbol{\nu}^2$. Since the difference of two convex functions is generally non-convex, the optimization problem is non-convex. Given that $\mathcal{D}_k(\boldsymbol{\nu})$ is a sum of squared terms, we define a vector [5]

$$\mathbf{f}_k(\boldsymbol{\nu}) = \begin{bmatrix} \{\nu_{k'0} B_{k0,k'}, \nu_{k'l} B_{kl,k'}\}_{k' \in \mathcal{P}_k \setminus \{k\}, l \in \mathbb{L}} \\ \{\nu_{k'0} C_{k0,k'}, \nu_{k'l} C_{kl,k'}\}_{k' \in \mathbb{K}, l \in \mathbb{L}} \\ \sigma_z \end{bmatrix}, \quad (43)$$

such that $\|\mathbf{f}_k(\boldsymbol{\nu})\|^2 = \mathcal{D}_k(\boldsymbol{\nu})$. Finally, the constraint (C1) is reformulated as

$$\nu_{k0} A_{k0} + \sum_{l \in \mathbb{L}} \nu_{kl} A_{kl} \geq \sqrt{\xi_t} \|\mathbf{f}_k(\boldsymbol{\nu})\|, \quad (44)$$

which is a standard second-order cone constraint. This transformation converts the problem into a convex form, allowing it to be efficiently solved through a sequence of convex feasibility problems. To solve it, we present a bisection method, as detailed in Algorithm 2.

C. Cellular Massive MIMO

In the downlink of a cellular system, the BS transmits

$$\mathbf{s}_b = \sqrt{p_c} \sum_{k \in \mathbb{K}} \frac{\sqrt{\zeta_k} \hat{\mathbf{g}}_k^* u_k}{\sqrt{\mathbb{E}[\|\hat{\mathbf{g}}_k\|^2]}}, \quad (45)$$

Algorithm 2: Downlink Max-Min Power Control

Input: $\{\mathbf{R}_{k0}, \mathbf{R}_{kl}, \boldsymbol{\Gamma}_{k0}, \boldsymbol{\Gamma}_{kl}\}_{k \in \mathbb{K}, l \in \mathbb{L}}, p_u, p_a, p_b, \sigma_z^2, \epsilon$;

Output: Optimal power coefficients $\boldsymbol{\nu}^*$

Initialization:

$$t \leftarrow 0, \quad \xi_{\text{low}}^{(0)} \leftarrow 0$$

$$\xi_{\text{high}}^{(0)} \leftarrow \max \left\{ \frac{(A_{k0} + \sum_{l \in \mathbb{L}} A_{kl})^2}{\sigma_z^2} \right\}$$

$$\{A_{k0}, A_{kl}, B_{k0,k'}, B_{kl,k'}, C_{k0,k'}, C_{kl,k'}\}_{\forall k, k' \in \mathbb{K}, l \in \mathbb{L}}$$

while $\xi_{\text{high}}^{(t)} - \xi_{\text{low}}^{(t)} > \epsilon$ **do**

$$\xi_t \leftarrow \frac{1}{2} (\xi_{\text{low}}^{(t)} + \xi_{\text{high}}^{(t)})$$

Convex Feasibility Check:

Find $\boldsymbol{\nu}$

$$\begin{aligned} \text{s.t. } & \nu_{k0} A_{k0} + \sum_{l \in \mathbb{L}} \nu_{kl} A_{kl} \geq \sqrt{\xi_t} \|\mathbf{f}_k(\boldsymbol{\nu})\|, \quad \forall k \in \mathbb{K} \\ & \sum_{k \in \mathbb{K}} \nu_{k0}^2 \leq 1, \quad \sum_{k \in \mathbb{K}} \nu_{kl}^2 \leq 1, \quad \forall l \in \mathbb{L} \\ & \nu_{k0} \geq 0, \quad \nu_{kl} \geq 0, \quad \forall k \in \mathbb{K}, l \in \mathbb{L} \end{aligned}$$

if feasible then

$$\begin{aligned} & \xi_{\text{low}}^{(t+1)} \leftarrow \xi_t, \quad \xi_{\text{high}}^{(t+1)} \leftarrow \xi_{\text{high}}^{(t)} \\ & \boldsymbol{\nu}^* \leftarrow \boldsymbol{\nu} \end{aligned}$$

end

else

$$\begin{aligned} & \xi_{\text{low}}^{(t+1)} \leftarrow \xi_{\text{low}}^{(t)}, \quad \xi_{\text{high}}^{(t+1)} \leftarrow \xi_t \end{aligned}$$

end

$$t \leftarrow t + 1$$

end

return $\boldsymbol{\nu}^*$

where p_c is the BS power constraint and ζ_k denotes power coefficient assigned to user k . As a result, user k sees

$$y_k = \mathbf{g}_k^T \mathbf{s}_b + n_k \quad (46)$$

$$= \sqrt{p_c} \sum_{k' \in \mathbb{K}} \sqrt{\zeta_{k'}} \mathbf{g}_k^T \frac{\hat{\mathbf{g}}_{k'}^*}{\sqrt{\mathbb{E}[\|\hat{\mathbf{g}}_{k'}\|^2]}} u_{k'} + n_k.$$

Proposition 5. The downlink SE for user k in a cellular system, considering correlated channels and pilot contamination, is expressed as $C_k^c = \mathbb{E}[\log_2(1 + \xi_k^c)]$, where

$$\xi_k^c = \frac{p_u \tau_p \zeta_k \text{tr}(\mathbf{R}_k \boldsymbol{\Gamma}_k^{-1} \mathbf{R}_k)}{\left\{ \sum_{k' \in \mathcal{P}_k \setminus \{k\}} \zeta_{k'} \frac{p_u \tau_p |\text{tr}(\mathbf{R}_k \boldsymbol{\Gamma}_{k'}^{-1} \mathbf{R}_{k'})|^2}{\text{tr}(\mathbf{R}_{k'} \boldsymbol{\Gamma}_{k'}^{-1} \mathbf{R}_{k'})} \right\} + \sum_{k' \in \mathbb{K}} \zeta_{k'} \frac{\text{tr}(\mathbf{R}_k \mathbf{R}_{k'} \boldsymbol{\Gamma}_{k'}^{-1} \mathbf{R}_{k'})}{\text{tr}(\mathbf{R}_{k'} \boldsymbol{\Gamma}_{k'}^{-1} \mathbf{R}_{k'})} + \frac{\sigma_z^2}{p_c}}. \quad (47)$$

D. Cell-Free Massive MIMO

In the downlink of a CF system, AP a transmits

$$\mathbf{s}_a = \sqrt{p_a} \sum_{k \in \mathbb{K}} \frac{\sqrt{\zeta_{ka}} \hat{\mathbf{g}}_{ka}^* u_k}{\sqrt{\mathbb{E}[\|\hat{\mathbf{g}}_{ka}\|^2]}}, \quad (48)$$

where ζ_{ka} represents the power coefficient for AP a to user k . The observation at user k is given by $y_k = \sum_{a \in \mathbb{A}} \mathbf{g}_{ka}^T \mathbf{s}_a + n_k$, which can be further expanded as

$$y_k = \sqrt{p_a} \sum_{k' \in \mathbb{K}} \sum_{a \in \mathbb{A}} \sqrt{\zeta_{k'a}} \mathbf{g}_{ka}^T \frac{\hat{\mathbf{g}}_{k'a}^*}{\sqrt{\mathbb{E}[\|\hat{\mathbf{g}}_{k'a}\|^2]}} u_{k'} + n_k. \quad (49)$$

Proposition 6. *The downlink SE for user k in a cell-free system, considering correlated channels and pilot contamination, is expressed as $C_k^{cf} = \mathbb{E}[\log_2(1 + \xi_k^{cf})]$, where*

$$\xi_k^{cf} = \frac{p_u \tau_p \left| \sum_{a \in \mathbb{A}} \sqrt{\zeta_{ka} \text{tr}(\mathbf{R}_{ka} \mathbf{\Gamma}_{ka}^{-1} \mathbf{R}_{ka})} \right|^2}{\left\{ \sum_{k' \in \mathcal{P}_k \setminus \{k\}} \sum_{a \in \mathbb{A}} \frac{\zeta_{k'a} p_u \tau_p |\text{tr}(\mathbf{R}_{ka} \mathbf{\Gamma}_{k'a}^{-1} \mathbf{R}_{k'a})|^2}{\text{tr}(\mathbf{R}_{k'a} \mathbf{\Gamma}_{k'a}^{-1} \mathbf{R}_{k'a})} \right\} + \sum_{k' \in \mathbb{K}} \sum_{a \in \mathbb{A}} \frac{\zeta_{k'a} \text{tr}(\mathbf{R}_{ka} \mathbf{R}_{k'a} \mathbf{\Gamma}_{k'a}^{-1} \mathbf{R}_{k'a})}{\text{tr}(\mathbf{R}_{k'a} \mathbf{\Gamma}_{k'a}^{-1} \mathbf{R}_{k'a})} + \frac{\sigma_z^2}{p_a}}. \quad (50)$$

VI. PERFORMANCE EVALUATION

A numerical evaluation of the proposed HCF architecture is conducted, benchmarking its performance against CF and cellular systems with respect to both worst-case per-user SE and overall system capacity. Additionally, the results regarding the reduction in fronthaul costs and the saving of transmission power are presented.

A. Simulation Configuration

In our simulations, we examine two representative scenarios: a compact area reflecting a microcell-scale scenario and a larger area representing a macrocell-scale environment.

Microcell Scenario: A circular area with a 500-meter radius, consistent with the 3GPP Urban Microcell model, applies a path loss model:

$$\beta = -30.5 - 36.7 \lg(d) + \mathcal{X}, \quad (51)$$

where d is the propagation distance in meters, and shadowing \mathcal{X} follows $\mathcal{N}(0, \sigma_{sd}^2)$ with standard derivation $\sigma_{sd} = 4$ dB. The system deploys a total of $M = 128$ antennas to serve $K = 8$ active users. To implement HCF, by default, one-quarter of the antennas ($N_b = 32$) are allocated to the cBS, along with 24 eAPs, each equipped with four antennas, are uniformly distributed throughout the coverage area. This configuration reduces the fronthaul network scale by 25%, resulting in equivalent reductions in hardware costs and signaling overhead. We employ an HCF variant by increasing antenna centralization to half. In HCF-1/2, 64 co-located antennas are placed at the cBS, with 16 four-antenna eAPs. This setup further reduces the fronthaul scale to 50% of the original CF network. For a fair comparison, all network configurations maintain the same number of antennas. Thus, the CF system consists of 32 distributed APs, each equipped with four antennas, whereas in the cellular case, a BS with 128 co-located antennas is used. At each simulation epoch, the locations of APs/eAPs and users are randomly varied.

Macrocell Scenario: The coverage radius extends to 2km with $M = 384$ antennas serving $K = 16$ active users. The antenna distribution mirrors that of the microcell scenario, with each AP/eAP equipped with four antennas. The large-scale fading is given by $\beta = 10^{\frac{L+\mathcal{X}}{10}}$, where the shadowing $\mathcal{X} \sim \mathcal{N}(0, 8^2)$, and path loss uses the COST-Hata model [5]:

$$\mathcal{L} = \begin{cases} -L_0 - 35 \lg(d), & d > d_1 \\ -L_0 - 10 \lg(d_1^{1.5} d^2), & d_0 < d \leq d_1 \\ -L_0 - 10 \lg(d_1^{1.5} d_0^2), & d \leq d_0 \end{cases}, \quad (52)$$

where the three-slope breakpoints take values $d_0 = 10$ m and $d_1 = 50$ m while $L_0 = 140.72$ dB in terms of

$$L_0 = 46.3 + 33.9 \lg(f_c) - 13.82 \lg(h_{eAP}) - [1.1 \lg(f_c) - 0.7] h_{UE} + 1.56 \lg(f_c) - 0.8 \quad (53)$$

with carrier frequency $f_c = 1.9$ GHz, the height of eAP antenna $h_{eAP} = 15$ m, and the height of UE $h_{UE} = 1.65$ m.

General Parameters: The UE transmit power is limited to $p_u = 200$ mW. Each antenna has a power constraint of 50mW, meaning that a BS with 384 antennas can transmit up to 19.2W, while each AP is restricted to a maximum power of 200mW. The system operates with a noise power spectral density of -174 dBm/Hz, a 9dB noise figure, and a bandwidth of 5MHz. All antenna arrays are configured as half-wavelength-spaced uniform linear arrays. We simulate spatial correlation using the Gaussian local scattering model [30, Sec. 2.6], applying an angular standard deviation of 10° for macrocell scenarios and 30° for microcell scenarios. Each coherence block contains $\tau_c = 200$ channel uses (e.g., achieved by 2ms coherence time and 100kHz coherence bandwidth). Without loss of generality, we set the length of the pilot sequence to half the total number of active users, i.e., $\tau_p = 4$ and 8 in the microcell and macrocell scenarios, respectively. This implies that every two users share a pilot sequence, leading to pilot contamination.

B. Numerical Results

We begin by examining the downlink performance in a microcell scenario, comparing the cumulative distribution functions (CDFs) of per-user SE for HCF, CF, and cellular (cel) networks, under both equal and max-min power control, as illustrated in Fig.2a. The 95%-likely user rate, as a key indicator for cell-edge performance, corresponds to the 5th percentile of these CDF curves. HCF (default with 1/4 antenna aggregation) achieves a 95%-likely rate of 0.65bps/Hz. This result outperforms CF (0.61bps/Hz), and demonstrates a 50-fold improvement compared to cellular (0.013bps/Hz). Max-min power control significantly boosts performance for distributed architectures: CF-maxmin reaches 2.05bps/Hz, while HCF-maxmin achieves 2.03bps/Hz. In cellular systems, the 95%-likely rate degrades under max-min power control (0.006bps/Hz vs. 0.013bps/Hz). This happens because the majority of the total power—sometimes over 90%—is assigned to a cell-edge user with the weakest channel, leaving very little power for cell-center users with stronger channels. Such extreme power redistribution is highly inefficient. Power

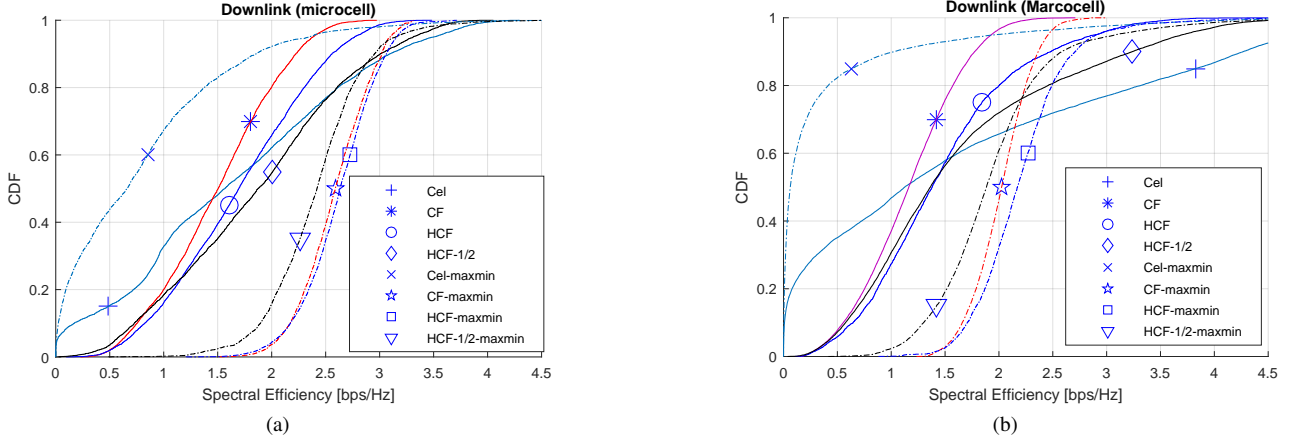


Fig. 2. Downlink performance comparison of HCF, CF, and cellular systems in (a) microcell and (b) macrocell under equal and max-min power control.

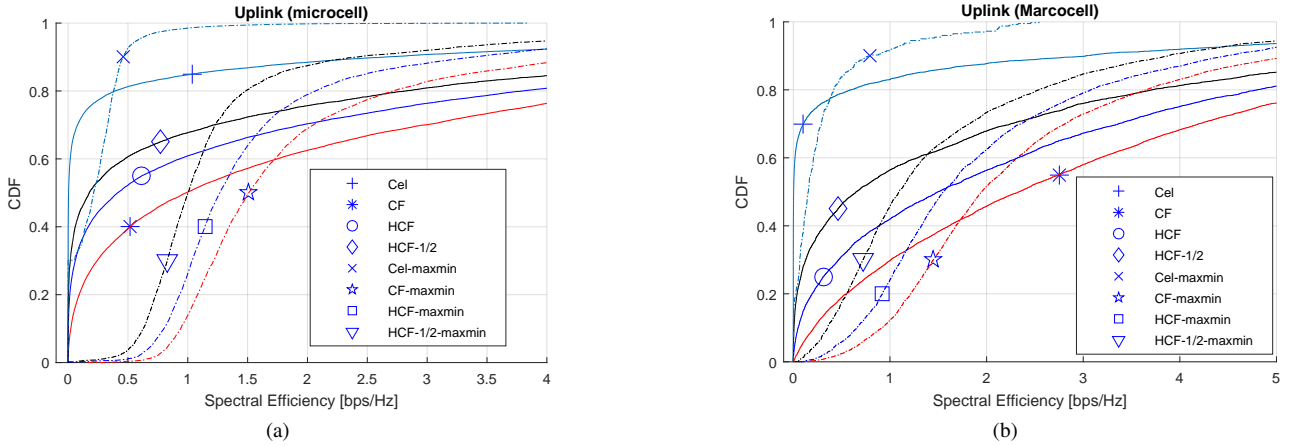


Fig. 3. Uplink performance comparison of HCF, CF, and cellular systems in (a) microcell and (b) macrocell under **full power** and max-min power control.

control operates differently in HCF: each distributed eAP independently allocates most of its power to its own worst-connected users without affecting other eAPs. This localized optimization ensures fairness without sacrificing overall performance. The effect of HCF's antenna aggregation are further examined. Increasing centralization to HCF-1/2 (half of antennas aggregated centrally) reduces the results under equal power (0.55bps/Hz vs. 0.65bps/Hz for default HCF). However, it reduces fronthaul cost and signaling overhead by roughly 50% (compared to 25% savings for default HCF). Applying max-min to HCF-1/2 recovers significant fairness (1.72bps/Hz), though it remains below CF-maxmin, illustrating its balance between centralization benefits (cost savings) and distributed gains (fairness).

In our extended evaluation, as shown in Fig.2b, we evaluated downlink performance in a macrocell scenario. As expected, user rates declined compared to that of microcell due to larger propagation loss. HCF achieves 0.46 bps/Hz, outperforming cellular (0.0017) and CF (0.42 bps/Hz), reaffirming its superiority in large-coverage cases. Max-min power control significantly enhances fairness of HCF systems to 1.59 bps/Hz, surpassing even CF-maxmin (1.56 bps/Hz). Conversely, cellular systems exhibit performance degradation

under max-min (less than 0.001 vs. 0.0017 bps/Hz), as extreme inefficient power allocation to cell-edge users starves cell-center users. For HCF-1/2, 95%-likely rate declines under equal power (0.43 vs. 0.46 bps/Hz for default HCF). Applying max-min to HCF-1/2 partially recovers fairness (1.15 bps/Hz) but remains below CF-maxmin. The proposed max-min power control not only enhances performance but also effectively reduces transmission power. Specifically, it achieves a **10.67%** reduction in power at the cBS and an average reduction of **23.51%** in power usage for eAPs.

The simulation results for uplink microcell scenarios is given in Fig.3a. Cellular networks exhibit poor performance, highlighting the inefficiency of traditional cellular systems for edge users. In contrast, CF and HCF demonstrate vast superiority, particularly with max-min power control, achieving 95%-likely user rates of 0.83 and 0.70 bps/Hz, respectively. While HCF loses some worst-case performance compared to CF, it still substantially outperforms the cellular network. Importantly, HCF achieves high fairness while reducing fronthaul scale and signaling overhead by approximately 25%. HCF-1/2 trades additional performance for even greater cost efficiency, showing further rate loss (with a 95%-likely rate of 0.54 bps/Hz), but achieving an impressive 50% reduction

in fronthaul network, making it a highly cost-effective alternative.

Max-min power control across users is highly effective, not only enhancing performance but also substantially reducing the transmission power, **compared with the full power transmission of UEs**. Fig.4 illustrates the variation in optimal coefficients across 30 independent power control trials. The Y-axis represents the power coefficient, ranging from 0 to 1, while the X-axis corresponds to independent power control instances over different simulation epoch, where user locations are randomly varied. Each box plot features a central line indicating the median, box edges marking the 25th and 75th percentiles, and a cross symbol representing the peak transmission power among users. The data reveals that while the worst-performing users transmit almost full power, the majority of users operate at lower power levels. Aggregating results from 2000 epochs, the proposed max-min algorithm saves approximately **73%** power, **compared with simply using full power in the uplink**. This is particularly advantageous for battery-powered mobile terminals, extending their operational lifetime.

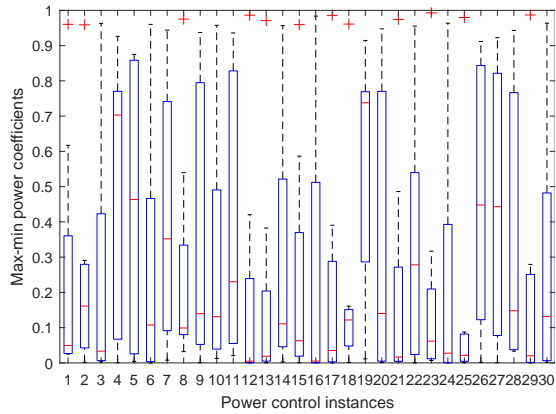


Fig. 4. Variations in optimal max-min power coefficients.

The simulation results for uplink macrocell scenarios, as illustrated in Fig.3b, demonstrate performance trends consistent with those observed in microcell environments. The proposed hierarchical architecture achieves a 95%-likely rate of 0.015 bps/Hz under equal power conditions, which is lower than that of CF but still significantly outperforms cellular networks. Increasing centralization to HCF-1/2 leads to a performance decline to below 0.002 bps/Hz. This highlights the important role of distributed APs in promoting fairness. Implementing max-min power control within the HCF and HCF-1/2 enhances performance to 0.45 bps/Hz and 0.23 bps/Hz, respectively, partially restoring the fairness observed in CF (0.68 bps/Hz). Notably, max-min power control reduces the transmission power of user equipment by approximately **60.5%** in this case.

In addition to fairness, overall system capacity serves as a critical performance metric. Fig.5 illustrates the CDFs of sum throughput for HCF, CF, and cellular networks under both equal and max-min power control in the downlink of a microcell scenario, as Fig.2a. The results reveal distinct

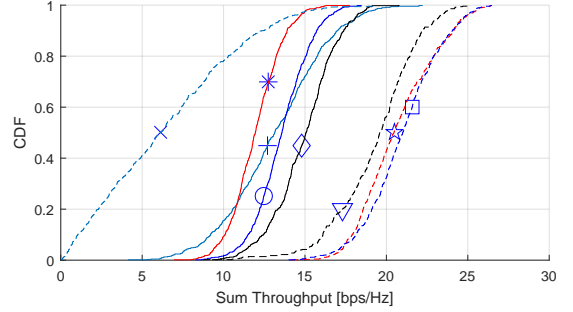


Fig. 5. System Capacity Comparison. Note that: marker identifiers align with those in previous figures.

trade-offs: cellular systems, despite their severe cell-edge performance limitations, achieve high sum throughput due to the exceptional QoS experienced by cell-center users. Conversely, fully distributed CF networks prioritize fairness at the expense of lower sum throughput. HCF, particularly HCF-1/2, strike a balance by leveraging cBS to maintain high QoS for cell-center users while deploying eAPs to enhance fairness. Our approach optimizes both fairness and system capacity while minimizing fronthaul infrastructure demands. Under max-min power control, as expected, cellular networks suffer substantial performance degradation due to inefficient power allocation. Although max-min power control improves CF network throughput, HCF consistently outperform CF, demonstrating superior capacity-fairness trade-offs.

VII. CONCLUSION

Traditional cellular systems suffer from severe performance degradation for cell-edge users, while fully distributed cell-free systems impose high fronthaul complexity and costs. This work introduces a hierarchical cell-free massive MIMO design, which aggregates a subset of antennas at a central base station while retaining some edge access points, thereby reducing fronthaul scale. Numerical results demonstrate that HCF ensures fairness, achieving a 95%-likely per-user spectral efficiency comparable to CF while significantly outperforming cellular networks. In addition to offering uniform quality of service, HCF preserves the benefits of centralization—e.g., HCF-1/2 reduces fronthaul scale by 50% while getting much higher system capacity than CF. Furthermore, the proposed max-min algorithms not only enhance fairness and system capacity but also substantially save power—particularly attractive for battery-powered user devices.

APPENDIX A EXPECTATIONS UNDER PILOT CONTAMINATION

The calculations for $\mathbb{E}[|\mathbf{h}_{kl}^T \hat{\mathbf{h}}_{k'l}^*|^2]$ vary depending on whether user k' shares the pilot sequence of user k . For $k' \notin$

\mathcal{P}_k , \mathbf{h}_{kl} and $\hat{\mathbf{h}}_{k'l}$ are *independent* because of $\mathbb{E}[\mathbf{i}_k^H \mathbf{i}_{k'}] = 0$. Thus, we have

$$\begin{aligned}\mathbb{E}[|\mathbf{h}_{kl}^T \hat{\mathbf{h}}_{k'l}^*|^2] &= \mathbb{E}[\mathbf{h}_{kl}^T \hat{\mathbf{h}}_{k'l}^* \hat{\mathbf{h}}_{k'l}^T \mathbf{h}_{kl}^*] \\ &= \text{tr} \left(\mathbb{E}[\mathbf{h}_{kl}^* \mathbf{h}_{kl}^T] \mathbb{E}[\hat{\mathbf{h}}_{k'l}^* \hat{\mathbf{h}}_{k'l}^T] \right) \\ &= p_u \tau_p \text{tr} \left(\mathbf{R}_{kl} \mathbf{R}_{k'l} \mathbf{\Gamma}_{k'l}^{-1} \mathbf{R}_{k'l} \right),\end{aligned}\quad (54)$$

due to $\mathbb{E}[\mathbf{h}_{kl} \mathbf{h}_{kl}^H] = \mathbf{R}_{kl}$ and $\mathbb{E}[\hat{\mathbf{h}}_{k'l} \hat{\mathbf{h}}_{k'l}^H] = p_u \tau_p \mathbf{R}_{k'l} \mathbf{\Gamma}_{k'l}^{-1} \mathbf{R}_{k'l}$ see (8). In contrast, \mathbf{h}_{kl} and $\hat{\mathbf{h}}_{k'l}$ are *correlated* for $k' \in \mathcal{P}_k$ (including k) due to pilot contamination caused by the shared pilot sequence. Consequently, the mathematical expectation becomes *non-multiplicative*, where $\mathbb{E}[X_1 X_2] \neq \mathbb{E}[X_1] \mathbb{E}[X_2]$ for two correlated random variables X_1 and X_2 . Thus,

$$\begin{aligned}\mathbb{E}[|\mathbf{h}_{kl}^T \hat{\mathbf{h}}_{k'l}^*|^2] &= \mathbb{E}[(\hat{\mathbf{h}}_{kl}^T + \tilde{\mathbf{h}}_{kl}^T) \hat{\mathbf{h}}_{k'l}^* \hat{\mathbf{h}}_{k'l}^T (\hat{\mathbf{h}}_{kl}^* + \tilde{\mathbf{h}}_{kl}^*)] \\ &= \underbrace{\mathbb{E}[\hat{\mathbf{h}}_{kl}^T \hat{\mathbf{h}}_{k'l}^* \hat{\mathbf{h}}_{k'l}^T \hat{\mathbf{h}}_{kl}^*]}_{\mathcal{F}_1} + \underbrace{\mathbb{E}[\tilde{\mathbf{h}}_{kl}^T \hat{\mathbf{h}}_{k'l}^* \hat{\mathbf{h}}_{k'l}^T \tilde{\mathbf{h}}_{kl}^*]}_{\mathcal{F}_2},\end{aligned}\quad (55)$$

where the two cross terms vanish due to $\mathbb{E}[\hat{\mathbf{h}}_{kl}^H \tilde{\mathbf{h}}_{kl}] = 0$.

Recalling (6), we have $\hat{\mathbf{h}}_{kl} = \sqrt{p_u} \mathbf{R}_{kl} \mathbf{\Gamma}_{kl}^{-1} \psi_{kl}$, and similarly $\hat{\mathbf{h}}_{k'l} = \sqrt{p_u} \mathbf{R}_{k'l} \mathbf{\Gamma}_{k'l}^{-1} \psi_{kl}$. Here, $\mathbf{\Gamma}_{k'l} = \mathbf{\Gamma}_{kl}$ and $\psi_{k'l} = \psi_{kl}$ because of the shared pilot sequence. Referring to Corollary 4.5 of [30], \mathcal{F}_1 in (55) becomes

$$\begin{aligned}\mathcal{F}_1 &= \mathbb{E}[|\hat{\mathbf{h}}_{k'l}^H \hat{\mathbf{h}}_{kl}|^2] = p_u^2 \mathbb{E}[|\psi_{kl}^H \mathbf{\Gamma}_{kl}^{-1} \mathbf{R}_{k'l} \mathbf{R}_{kl} \mathbf{\Gamma}_{kl}^{-1} \psi_{kl}|^2] \\ &= p_u^2 \tau_p^2 |\text{tr}(\mathbf{\Gamma}_{kl}^{-1} \mathbf{R}_{k'l} \mathbf{R}_{kl} \mathbf{\Gamma}_{kl}^{-1})|^2 \\ &\quad + p_u^2 \tau_p^2 \text{tr}(\mathbf{\Gamma}_{kl}^{-1} \mathbf{R}_{k'l} \mathbf{R}_{kl} \mathbf{\Gamma}_{kl}^{-1} \mathbf{\Gamma}_{kl} \mathbf{\Gamma}_{kl}^{-1} \mathbf{R}_{kl} \mathbf{R}_{k'l} \mathbf{\Gamma}_{kl}^{-1} \mathbf{\Gamma}_{kl}) \\ &= p_u^2 \tau_p^2 |\text{tr}(\mathbf{\Gamma}_{kl}^{-1} \mathbf{R}_{k'l} \mathbf{R}_{kl})|^2 \\ &\quad + p_u^2 \tau_p^2 \text{tr}(\mathbf{\Gamma}_{kl}^{-1} \mathbf{R}_{k'l} \mathbf{R}_{kl} \mathbf{\Gamma}_{kl}^{-1}) \\ &= p_u^2 \tau_p^2 |\text{tr}(\mathbf{R}_{kl} \mathbf{\Gamma}_{kl}^{-1} \mathbf{R}_{k'l})|^2 \\ &\quad + p_u \tau_p \text{tr}((\mathbf{R}_{kl} - \Theta_{kl}) \mathbf{R}_{k'l} \mathbf{\Gamma}_{kl}^{-1} \mathbf{R}_{k'l}).\end{aligned}\quad (56)$$

The above derivation relies on the fact that \mathbf{R}_{kl} , for any k , is a Hermitian matrix, i.e., $\mathbf{R}_{kl} = \mathbf{R}_{kl}^H$, and the cyclic property of the trace operation, which allows

$$\text{tr}(\mathbf{R}_{kl} \mathbf{\Gamma}_{kl}^{-1} \mathbf{R}_{k'l}) = \text{tr}(\mathbf{\Gamma}_{kl}^{-1} \mathbf{R}_{k'l} \mathbf{R}_{kl}) = \text{tr}(\mathbf{R}_{k'l} \mathbf{R}_{kl} \mathbf{\Gamma}_{kl}^{-1}). \quad (57)$$

The second term \mathcal{F}_2 in (55) becomes

$$\begin{aligned}\mathcal{F}_2 &= \mathbb{E}[\tilde{\mathbf{h}}_{kl}^H \hat{\mathbf{h}}_{k'l} \hat{\mathbf{h}}_{k'l}^H \tilde{\mathbf{h}}_{kl}] = \text{tr} \left(\mathbb{E}[\tilde{\mathbf{h}}_{kl} \tilde{\mathbf{h}}_{kl}^H] \mathbb{E}[\hat{\mathbf{h}}_{k'l} \hat{\mathbf{h}}_{k'l}^H] \right) \\ &= p_u \tau_p \text{tr}(\Theta_{kl} \mathbf{R}_{k'l} \mathbf{\Gamma}_{k'l}^{-1} \mathbf{R}_{k'l}).\end{aligned}\quad (58)$$

Substituting (56) and (58) into (55), yield

$$\begin{aligned}\mathbb{E}[|\mathbf{h}_{kl}^T \hat{\mathbf{h}}_{k'l}^*|^2] &= p_u^2 \tau_p^2 |\text{tr}(\mathbf{R}_{kl} \mathbf{\Gamma}_{k'l}^{-1} \mathbf{R}_{k'l})|^2 \\ &\quad + p_u \tau_p \text{tr}(\mathbf{R}_{kl} \mathbf{R}_{k'l} \mathbf{\Gamma}_{k'l}^{-1} \mathbf{R}_{k'l}).\end{aligned}\quad (59)$$

This result is also applied for \mathbf{h}_{k0} and $\hat{\mathbf{h}}_{k'0}$, we obtain

$$\mathbb{E}[|\mathbf{h}_{k0}^T \hat{\mathbf{h}}_{k'0}^*|^2] = \begin{cases} p_u \tau_p \text{tr}(\mathbf{R}_{k0} \mathbf{R}_{k'0} \mathbf{\Gamma}_{k'0}^{-1} \mathbf{R}_{k'0}), & k' \notin \mathcal{P}_k \\ p_u^2 \tau_p^2 |\text{tr}(\mathbf{R}_{k0} \mathbf{\Gamma}_{k'0}^{-1} \mathbf{R}_{k'0})|^2 + p_u \tau_p \text{tr}(\mathbf{R}_{k0} \mathbf{R}_{k'0} \mathbf{\Gamma}_{k'0}^{-1} \mathbf{R}_{k'0}), & k' \in \mathcal{P}_k \end{cases} \quad (60)$$

APPENDIX B PROOF OF PROPOSITION 4.

Referring to (19), the downlink SINR of HCF is given by

$$\xi_k^{hcf} = \frac{|\mathcal{S}_1|^2}{\mathbb{E}[|\mathcal{J}_1 + \mathcal{J}_2|^2] + \sigma_z^2}, \quad (61)$$

where the power gain of u_k equals

$$|\mathcal{S}_1|^2 = \left| \sqrt{p_b \eta_{k0} \mathbb{E}[|\hat{\mathbf{h}}_{k0}|^2]} + \sum_{l \in \mathbb{L}} \sqrt{p_a \eta_{kl} \mathbb{E}[|\hat{\mathbf{h}}_{kl}|^2]} \right|^2. \quad (62)$$

The expected power of $\hat{\mathbf{h}}_{kl}$ is

$$\mathbb{E}[|\hat{\mathbf{h}}_{kl}|^2] = \text{tr} \left(\mathbb{E} \left[\hat{\mathbf{h}}_{kl} \hat{\mathbf{h}}_{kl}^H \right] \right) = p_u \tau_p \text{tr}(\mathbf{R}_{kl} \mathbf{\Gamma}_{kl}^{-1} \mathbf{R}_{kl}), \quad (63)$$

following from (8). Similarly, for $\hat{\mathbf{h}}_{k0}$, we have

$$\mathbb{E}[|\hat{\mathbf{h}}_{k0}|^2] = p_u \tau_p \text{tr}(\mathbf{R}_{k0} \mathbf{\Gamma}_{k0}^{-1} \mathbf{R}_{k0}), \quad (64)$$

since $\mathbb{E}[\hat{\mathbf{h}}_{k0} \hat{\mathbf{h}}_{k0}^H] = p_u \tau_p \mathbf{R}_{k0} \mathbf{\Gamma}_{k0}^{-1} \mathbf{R}_{k0}$, as derived from (12). Thus,

$$|\mathcal{S}_1|^2 = \left| \sqrt{p_b \eta_{k0} p_u \tau_p \text{tr}(\mathbf{R}_{k0} \mathbf{\Gamma}_{k0}^{-1} \mathbf{R}_{k0})} + \sum_{l \in \mathbb{L}} \sqrt{p_a \eta_{kl} p_u \tau_p \text{tr}(\mathbf{R}_{kl} \mathbf{\Gamma}_{kl}^{-1} \mathbf{R}_{kl})} \right|^2. \quad (65)$$

Due to the independence of data symbols, i.e., $\mathbb{E}[u_k^* u_{k'}] = 0$ for $k' \neq k$, \mathcal{J}_1 and \mathcal{J}_2 in (37) are uncorrelated. This implies that $\mathbb{E}[|\mathcal{J}_1 + \mathcal{J}_2|^2] = \mathbb{E}[|\mathcal{J}_1|^2] + \mathbb{E}[|\mathcal{J}_2|^2]$. We now compute the variance of \mathcal{J}_1 as

$$\begin{aligned}\mathbb{E}[|\mathcal{J}_1|^2] &= \frac{p_b \eta_{k0} \mathbb{E} \left[\overbrace{\left| \hat{\mathbf{h}}_{k0}^T \hat{\mathbf{h}}_{k0} - \mathbb{E}[|\hat{\mathbf{h}}_{k0}|^2] \right|^2}^{\mathcal{T}_1} \right]}{\mathbb{E}[|\hat{\mathbf{h}}_{k0}|^2]} \\ &\quad + p_a \sum_{l \in \mathbb{L}} \frac{\eta_{kl} \mathbb{E} \left[\overbrace{\left| \hat{\mathbf{h}}_{kl}^T \hat{\mathbf{h}}_{kl} - \mathbb{E}[|\hat{\mathbf{h}}_{kl}|^2] \right|^2}^{\mathcal{T}_2} \right]}{\mathbb{E}[|\hat{\mathbf{h}}_{kl}|^2]}.\end{aligned}\quad (66)$$

The first term \mathcal{T}_1 in (66) is further derived as

$$\begin{aligned}\mathcal{T}_1 &= \mathbb{E} \left[\left| \hat{\mathbf{h}}_{k0}^T \hat{\mathbf{h}}_{k0} \right|^2 \right] - \mathbb{E} \left[\hat{\mathbf{h}}_{k0}^T \hat{\mathbf{h}}_{k0} \right] \mathbb{E}[|\hat{\mathbf{h}}_{k0}|^2] \\ &\quad - \mathbb{E} \left[\hat{\mathbf{h}}_{k0}^H \hat{\mathbf{h}}_{k0} \right] \mathbb{E}[|\hat{\mathbf{h}}_{k0}|^2] + \left(\mathbb{E}[|\hat{\mathbf{h}}_{k0}|^2] \right)^2 \\ &= \mathbb{E} \left[\left| \hat{\mathbf{h}}_{k0}^T \hat{\mathbf{h}}_{k0} \right|^2 \right] - \mathbb{E} \left[(\hat{\mathbf{h}}_{k0}^T + \tilde{\mathbf{h}}_{k0}^T) \hat{\mathbf{h}}_{k0} \right] \mathbb{E}[|\hat{\mathbf{h}}_{k0}|^2] \\ &\quad - \mathbb{E} \left[(\hat{\mathbf{h}}_{k0}^H + \tilde{\mathbf{h}}_{k0}^H) \hat{\mathbf{h}}_{k0} \right] \mathbb{E}[|\hat{\mathbf{h}}_{k0}|^2] + \left(\mathbb{E}[|\hat{\mathbf{h}}_{k0}|^2] \right)^2 \\ &\stackrel{(a)}{=} \mathbb{E} \left[\left| \hat{\mathbf{h}}_{k0}^T \hat{\mathbf{h}}_{k0} \right|^2 \right] - \left(\mathbb{E}[|\hat{\mathbf{h}}_{k0}|^2] \right)^2.\end{aligned}\quad (67)$$

The derivation in step (a) relies on the independence between a channel estimate and its estimation error, namely $\mathbb{E}[\hat{\mathbf{h}}_{k0}^H \hat{\mathbf{h}}_{k0}] = 0$. From (60) in Appendix (A), we have

$$\begin{aligned}\mathbb{E}[|\hat{\mathbf{h}}_{k0}^T \hat{\mathbf{h}}_{k0}|^2] &= p_u^2 \tau_p^2 \left(\text{tr}(\mathbf{R}_{k0} \mathbf{\Gamma}_{k0}^{-1} \mathbf{R}_{k0}) \right)^2 \\ &\quad + p_u \tau_p \text{tr}(\mathbf{R}_{k0} \mathbf{R}_{k0} \mathbf{\Gamma}_{k0}^{-1} \mathbf{R}_{k0}).\end{aligned}\quad (68)$$

Substituting (64) and (68) into (67), \mathcal{T}_1 becomes

$$\mathcal{T}_1 = p_u \tau_p \text{tr}(\mathbf{R}_{k0} \mathbf{R}_{k0} \mathbf{\Gamma}_{k0}^{-1} \mathbf{R}_{k0}). \quad (69)$$

Similarly,

$$\mathcal{T}_2 = p_u \tau_p \text{tr}(\mathbf{R}_{kl} \mathbf{R}_{kl} \mathbf{\Gamma}_{kl}^{-1} \mathbf{R}_{kl}). \quad (70)$$

Using (63), (64), along with the expressions of \mathcal{T}_1 and \mathcal{T}_2 , the following result is obtained:

$$\begin{aligned} \mathbb{E} [|\mathcal{J}_1|^2] &= \frac{p_b \eta_{k0} \text{tr}(\mathbf{R}_{k0} \mathbf{R}_{k0} \mathbf{\Gamma}_{k0}^{-1} \mathbf{R}_{k0})}{\text{tr}(\mathbf{R}_{k0} \mathbf{\Gamma}_{k0}^{-1} \mathbf{R}_{k0})} \\ &\quad + p_a \sum_{l \in \mathbb{L}} \frac{\eta_{kl} \text{tr}(\mathbf{R}_{kl} \mathbf{R}_{kl} \mathbf{\Gamma}_{kl}^{-1} \mathbf{R}_{kl})}{\text{tr}(\mathbf{R}_{kl} \mathbf{\Gamma}_{kl}^{-1} \mathbf{R}_{kl})}. \end{aligned} \quad (71)$$

Next, the variance of \mathcal{J}_2 is computed as

$$\begin{aligned} \mathbb{E} [|\mathcal{J}_2|^2] &= p_b \sum_{k' \in \mathbb{K} \setminus \{k\}} \frac{\eta_{k'0} \mathbb{E} [|\mathbf{h}_{k'0}^T \hat{\mathbf{h}}_{k'0}^*|^2]}{\mathbb{E} [|\hat{\mathbf{h}}_{k'0}|^2]} \\ &\quad + p_a \sum_{k' \in \mathbb{K} \setminus \{k\}} \sum_{l \in \mathbb{L}} \frac{\eta_{k'l} \mathbb{E} [|\mathbf{h}_{kl}^T \hat{\mathbf{h}}_{k'l}^*|^2]}{\mathbb{E} [|\hat{\mathbf{h}}_{k'l}|^2]}. \end{aligned} \quad (72)$$

Based on the presence of pilot contamination, the set $\mathbb{K} \setminus \{k\}$ is divided into two non-overlapped subsets: $\mathcal{P}_k \setminus \{k\}$ and $\mathbb{K} \setminus \mathcal{P}_k$. Applying (54), (59), (60), (63), and (64), the variance of \mathcal{J}_2 is obtained as

$$\begin{aligned} \mathbb{E} [|\mathcal{J}_2|^2] &= \\ & p_b \sum_{k' \in \mathcal{P}_k \setminus \{k\}} \frac{\eta_{k'0} \left\{ p_u \tau_p \left| \text{tr}(\mathbf{R}_{k0} \mathbf{\Gamma}_{k'0}^{-1} \mathbf{R}_{k'0}) \right|^2 \right. \\ & \quad \left. + \text{tr}(\mathbf{R}_{k0} \mathbf{R}_{k'0} \mathbf{\Gamma}_{k'0}^{-1} \mathbf{R}_{k'0}) \right\}}{\text{tr}(\mathbf{R}_{k'0} \mathbf{\Gamma}_{k'0}^{-1} \mathbf{R}_{k'0})} \\ & + p_b \sum_{k' \in \mathbb{K} \setminus \mathcal{P}_k} \frac{\eta_{k'0} \text{tr}(\mathbf{R}_{k0} \mathbf{R}_{k'0} \mathbf{\Gamma}_{k'0}^{-1} \mathbf{R}_{k'0})}{\text{tr}(\mathbf{R}_{k'0} \mathbf{\Gamma}_{k'0}^{-1} \mathbf{R}_{k'0})} \\ & + p_a \sum_{k' \in \mathcal{P}_k \setminus \{k\}} \sum_{l \in \mathbb{L}} \frac{\eta_{k'l} \left\{ p_u \tau_p \left| \text{tr}(\mathbf{R}_{kl} \mathbf{\Gamma}_{k'l}^{-1} \mathbf{R}_{k'l}) \right|^2 \right. \\ & \quad \left. + \text{tr}(\mathbf{R}_{kl} \mathbf{R}_{k'l} \mathbf{\Gamma}_{k'l}^{-1} \mathbf{R}_{k'l}) \right\}}{\text{tr}(\mathbf{R}_{k'l} \mathbf{\Gamma}_{k'l}^{-1} \mathbf{R}_{k'l})} \\ & + p_a \sum_{k' \in \mathbb{K} \setminus \mathcal{P}_k} \frac{\eta_{k'l} \text{tr}(\mathbf{R}_{kl} \mathbf{R}_{k'l} \mathbf{\Gamma}_{k'l}^{-1} \mathbf{R}_{k'l})}{\text{tr}(\mathbf{R}_{k'l} \mathbf{\Gamma}_{k'l}^{-1} \mathbf{R}_{k'l})} \end{aligned} \quad (73)$$

In final, substituting (65), (71), and (73) into (61), and rearranging the terms yields (33). The final derivation applies

$$\frac{|\text{tr}(\mathbf{R}_{kl} \mathbf{\Gamma}_{kl}^{-1} \mathbf{R}_{kl})|^2}{\text{tr}(\mathbf{R}_{kl} \mathbf{\Gamma}_{kl}^{-1} \mathbf{R}_{kl})} = |\text{tr}(\mathbf{R}_{kl} \mathbf{\Gamma}_{kl}^{-1} \mathbf{R}_{kl})|$$

given that $\text{tr}(\mathbf{R}_{kl} \mathbf{\Gamma}_{kl}^{-1} \mathbf{R}_{kl}) = \frac{\mathbb{E} [|\hat{\mathbf{h}}_{kl}|^2]}{p_u \tau_p} > 0$, recalling (63).

REFERENCES

- W. Jiang and H. D. Schotten, "Hierarchical cell-free massive MIMO for high capacity with simple implementation," in *Proc. 2024 IEEE Int. Commun. Conf. (ICC)*, Denver, USA, Jun. 2024.
- W. Jiang and B. Han, *Cellular Communication Networks and Standards: The Evolution from 1G to 6G*. Cham, Switzerland: Springer, 2024.
- ITU-R M.2410, "Minimum requirements related to technical performance for IMT-2020 radio interface(s)," ITU-R, Recommendation M.2410-0, Nov. 2017.
- E. Nayebi *et al.*, "Precoding and power optimization in cell-free massive MIMO systems," *IEEE Trans. Wireless Commun.*, vol. 16, no. 7, pp. 4445–4459, Jul. 2017.
- H. Q. Ngo *et al.*, "Cell-free massive MIMO versus small cells," *IEEE Trans. Wireless Commun.*, vol. 16, no. 3, pp. 1834–1850, Mar. 2017.
- W. Jiang and H. D. Schotten, "Cell-edge performance booster in 6G: Cell-free massive MIMO vs. reconfigurable intelligent surface," in *Proc. IEEE Eur. Conf. on Netw. and Commun. (EUCNC)*, Gothenburg, Sweden, Jun. 2023, pp. 1–6.
- W. Jiang *et al.*, "The road towards 6G: A comprehensive survey," *IEEE Open J. Commun. Society*, vol. 2, pp. 334–366, Feb. 2021.
- W. Jiang and F.-L. Luo, "Cellular and cell-free massive MIMO techniques in 6G," in *6G Key Technologies: A Comprehensive Guide*. New York, USA: John Wiley&Sons and IEEE Press, 2023, ch. 9.
- E. Björnson and L. Sanguinetti, "Scalable cell-free massive MIMO systems," *IEEE Trans. Commun.*, vol. 68, no. 7, pp. 4247–4261, Jul. 2020.
- G. Interdonato *et al.*, "Downlink training in cell-free massive MIMO: A blessing in disguise," *IEEE Trans. Wireless Commun.*, vol. 18, no. 11, pp. 5153 – 5169, Nov. 2019.
- H. Q. Ngo *et al.*, "On the total energy efficiency of cell-free massive MIMO," *IEEE Trans. Green Commun. Netw.*, vol. 2, no. 1, pp. 25–39, Mar. 2018.
- E. Björnson and L. Sanguinetti, "Making cell-free massive MIMO competitive with MMSE processing and centralized implementation," *IEEE Trans. Wireless Commun.*, vol. 19, no. 1, pp. 77 – 90, Jan. 2020.
- H. Masoumi and M. J. Emadi, "Performance analysis of cell-free massive MIMO system with limited fronthaul capacity and hardware impairments," *IEEE Trans. Wireless Commun.*, vol. 19, no. 2, pp. 1038–1052, Feb. 2020.
- L. Furtado *et al.*, "Cell-free massive MIMO deployments: Fronthaul topology options and techno-economic aspects," in *Proc. 16th Eur. Conf. Antennas Propag. (EuCAP)*, Madrid, Spain, Mar. 2022, pp. 1–5.
- S. Buzzi and C. D'Andrea, "Cell-free massive MIMO: User-centric approach," *IEEE Wireless Commun. Lett.*, vol. 6, no. 6, pp. 706–709, Dec. 2017.
- S. Buzzi *et al.*, "User-centric 5G cellular networks: Resource allocation and comparison with the cell-free massive MIMO approach," *IEEE Trans. Wireless Commun.*, vol. 19, no. 2, pp. 1250–1264, Feb. 2020.
- W. Jiang and H. D. Schotten, "Cost-effectiveness analysis and design of cost-efficient cell-free massive MIMO systems," in *Proc. IEEE Int. Symp. on Pers., Indoor and Mobile Radio Commun. (PIMRC)*, Valencia, Spain, Sep. 2024.
- U. Demirhan and A. Alkhateeb, "Enabling cell-free massive MIMO systems with wireless millimeter wave fronthaul," *IEEE Trans. Wireless Commun.*, vol. 21, no. 11, pp. 9482–9496, Nov. 2022.
- A. H. Jazi *et al.*, "Integrated access and backhaul (IAB) in cell-free massive MIMO systems," *IEEE Access*, vol. 11, pp. 71 658 – 71 667, Jul. 2023.
- W. Li, R. Zhang, J. Wang *et al.*, "A two-tier terahertz fronthaul scheme for indoor industrial cell-free massive MIMO networks," *IEEE Trans. Ind. Informat.*, vol. 19, no. 1, pp. 123–134, Jan. 2023.
- I.-s. Kim, M. Bennis, and J. Choi, "Cell-free mmwave massive MIMO systems with low-capacity fronthaul links and low-resolution ADC/DACs," *IEEE Trans. Wireless Commun.*, vol. 21, no. 7, pp. 4972–4986, Jul. 2022.
- P. Parida and H. S. Dhillon, "Cell-free massive MIMO with finite fronthaul capacity: A stochastic geometry perspective," *IEEE Trans. Wireless Commun.*, vol. 22, no. 3, pp. 1555–1572, Mar. 2022.
- S. Park, A. H. Gokceoglu, L. Wang, and O. Simeone, "Scalable multivariate fronthaul quantization for cell-free massive MIMO," *IEEE Trans. Wireless Commun.*, vol. 23, no. 8, pp. 5150–5164, Aug. 2024.
- V. Ranjbar *et al.*, "Cell-free massive MIMO with sequential fronthaul architecture and limited memory access points," *IEEE Trans. Commun.*, vol. 72, no. 12, pp. 7611 – 7626, Dec. 2024.
- M. Kim and J. Lee, "Meta-heuristic approach for fronthaul bit allocation in cell-free massive MIMO systems," *IEEE Commun. Lett.*, vol. 27, no. 4, pp. 1020–1024, Apr. 2023.
- U. Siddique, H. Tabassum, and E. Hossain, "Downlink spectrum allocation for in-band and out-band wireless backhauling of full-duplex small cells," *IEEE Trans. Commun.*, vol. 65, no. 11, pp. 4863–4877, Nov. 2017.
- T. L. Marzetta, "Noncooperative cellular wireless with unlimited numbers of base station antennas," *IEEE Trans. Wireless Commun.*, vol. 9, no. 11, pp. 3590 – 3600, Nov. 2010.
- K. Yu *et al.*, "Modeling of wide-band MIMO radio channels based on NLoS indoor measurements," *IEEE Trans. Veh. Technol.*, vol. 53, no. 3, pp. 655–665, May 2004.

- [29] O. Elijah *et al.*, “A comprehensive survey of pilot contamination in massive MIMO—5G system,” *IEEE Commun. Surveys Tuts.*, vol. 18, no. 2, pp. 905–923, 2nd Quarter 2016.
- [30] E. Björnson, J. Hoydis, and L. Sanguinetti, “Massive MIMO networks: Spectral, energy, and hardware efficiency,” *Foundations and Trends in Signal Processing*, vol. 11, no. 3-4, pp. 154–655, 2017.
- [31] B. Hassibi and B. Hochwald, “How much training is needed in multiple-antenna wireless links?” *IEEE Trans. Inf. Theory*, vol. 49, no. 4, pp. 951 – 963, Apr. 2003.
- [32] M. Bashar *et al.*, “On the uplink max–min SINR of cell-free massive MIMO systems,” *IEEE Trans. Wireless Commun.*, vol. 18, no. 4, pp. 2021–2036, Apr. 2019.
- [33] T. L. Marzetta, “Massive MIMO: An introduction,” *Bell Labs Technical J.*, vol. 20, pp. 11 – 22, Mar. 2015.
- [34] H. Q. Ngo and E. G. Larsson, “No downlink pilots are needed in TDD massive MIMO,” *IEEE Trans. Wireless Commun.*, vol. 16, no. 5, pp. 2921–2935, May 2017.